Supporting information file

Time-Dependent Density-Functional Theory for Modelling Solid-State Fluorescence Emission of Organic Multicomponent Crystals

Mihails Arhangelskis,[*a,b] *Dominik B. Jochym,*[c] *Leonardo Bernasconi,*[c] *Tomislav Friščić,*[b] *Andrew J. Morris,*[*d] *and William Jones*[a]

[a] Dr. M Arhangelskis, Dr. W. Jones, Department of Chemistry, University of Cambridge, Lensfield Road, Cambridge CB2 1EW, UK
[b] Dr. M Arhangelskis, Dr. Tomislav Friščić, Department of Chemistry, McGill University, 801 Sherbrooke St. W., Montreal H3A 0B8, Québec, Canada
[c] Dr. D. B. Jochym, Dr. L. Bernasconi, STFC Rutherford Appleton Laboratory, Didcot OX11 0QX, UK.
[d] Dr. A. J. Morris School of Metallurgy and Materials, University of Birmingham, Edgbaston, Birmingham B15 2TT, UK

Table of Contents

1. Periodic DFT calculations

All plane-wave DFT calculations were performed in CASTEP 7.0.3[1] using the norm-conserving OPIUM[2] pseudopotentials. Plane-wave cutoff was set to 750 eV, all other parameters were left at their default settings, unless otherwise stated. TD-DFT excitation energies were calculated using Davidson eigen-solver

1.1 Ground state geometry optimization

Experimentally determined structures[3] were optimized in preparation for the subsequent fluorescence calculations. During the calculations both atomic positions and unit cell parameters were optimized. Calculations were performed using the semi-local PBE functional, Monkhorst-Pack[4] k-point grid spacing was set to 0.03 $Å^{-1}$. Dispersion energy contribution was calculated using the semi-empirical G06 dispersion correction.[5] Convergence criteria were set as follows: energy tolerance 10^{-5} eV/atom, maximum atomic force 10^{-2} eV $Å^{-1}$, maximum atom displacement 10^{-3} Å and residual stress 0.05 GPa.

For each cocrystal coformer the geometry optimization was performed both for a triclinic and monoclinic unit cell, giving a total of eight geometry optimizations. In each case the experimentally observed structure was found to have a lower lattice energy (Table S1). The optimized crystal structures were used in all the subsequent calculations.

Table S1. Calculated lattice enthalpies of triclinic and monoclinic crystal structures. Energies for structures found experimentally are shown in bold. It is evident that experimental structures (triclinic for **A:1** and monoclinic for **A:2**, **A:3** and **A:4**) are lower in energy.

Cocrystal	absolute energy / eV		relative energy / kJ mol^{-1}	
	triclinic (Z=1)	monoclinic (Z=2)	triclinic	monoclinic
A:1	**-6126.866**	-12253.338	**0.000**	18.977
A:2	-8599.815	**-17200.095**	22.452	**0.000**
A:3	-8714.254	**-17429.105**	28.861	**0.000**
A:4	-9378.664	**-18757.641**	15.146	**0.000**

1.2 Calculation of the solid-state fluorescence spectra

1.2.1 Selection of the mean-value k-point

The implementation of TD-DFT in CASTEP is limited to a calculation with a single k-point, which is generally not sufficient for an adequate Brillouin zone sampling. A possible way to improve Brillouin zone sampling is to perform the calculations on supercells. The computational cost of such calculations, however, makes them impractical for computational screening of luminescent materials.

An alternative to the supercell approach is the calculation on a primitive cell with one specially chosen k-point that provides the most accurate description of the whole Brillouin zone. The position of such a mean-value k-point has been analytically derived for cubic and tetragonal cells.[6] For the monoclinic and triclinic cells, however, analytical derivation of the mean-value k-point is far more complicated, therefore we adopted a more empirical approach. Our aim was to derive a k-point that reproduces the splitting between occupied and unoccupied bands most accurately. This was achieved by calculating the Singlet-Triplet energy gap for a series of individual k-points and comparing these values to the converged k-point grid (0.03 $Å^{-1}$ spacing). The energies were calculated with the PBE functional. The k-point most closely matching the energy gap of the converged grid was used as the mean-value k-point. For the triclinic structure of **A:1** cocrystal the mean-value k-point was found at $(^1/_4, -^3/_8, ^1/_8)$, whilst the monoclinic structures **A:2**, **A:3** and **A:4** all had the mean-value k-point at$(-^1/_4, ^1/_4, ^3/_8)$. The summary of mean-value k-points is given in Tables S2-S5.

The advantage of using the mean-value k-point can be clearly seen by comparing the fluorescence spectra of **A:1** cocrystal calculated at the mean-value and gamma k-points (Figure S1). It is evident that the mean-value approach provides a far better agreement with experiment.

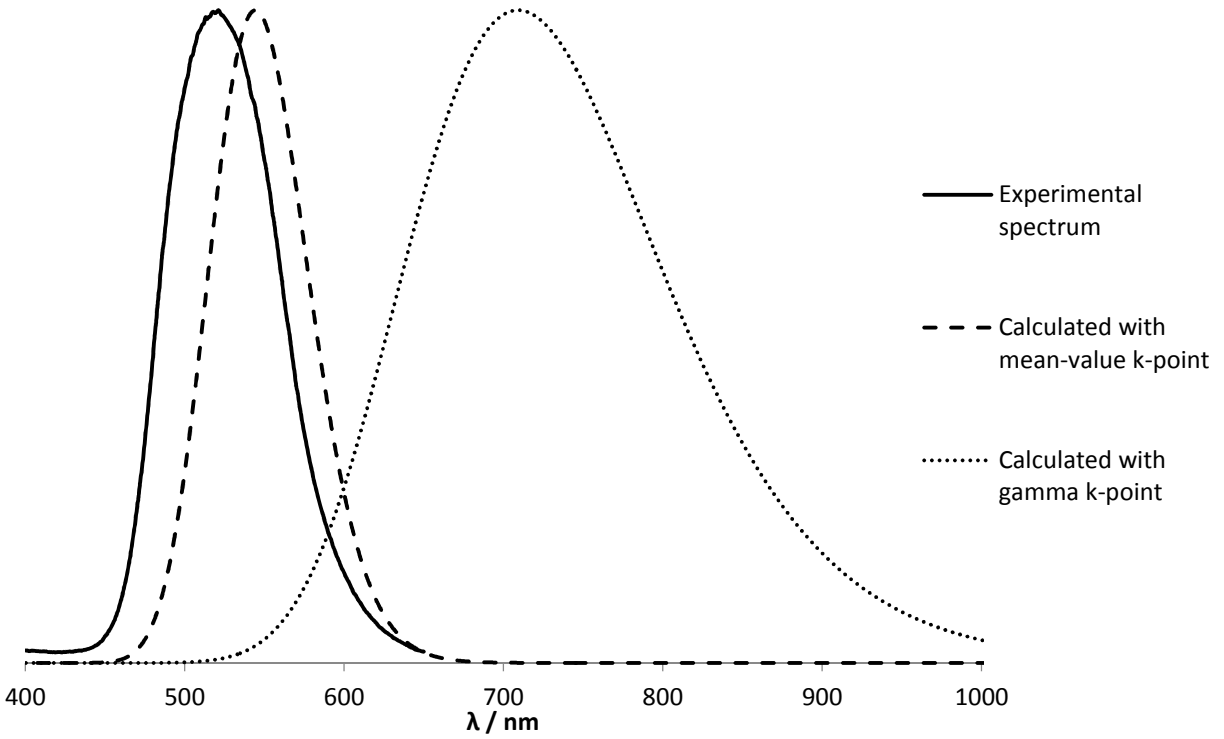

Figure S1. Comparison of the experimental and calculated spectra for the triclinic structure of cocrystal **A:1**. The experimental spectrum is shown with a solid line, the spectrum calculated using mean-value k-point is shown with a dashed line, while the dotted line represents calculation using the gamma k-point. The advantage of the mean-value approach is evident from a better agreement with experiment.

Table S2. Determination of the mean-value k-point for the triclinic structure of cocrystal **A:1**. The energies for the singlet, triplet and singlet-triplet gap of the converged k-point grid are -6122.429 eV, -6120.754 eV and 1.674 eV, respectively. The $(^1/_4, -^3/_8, ^1/_8)$ k-point, shown in red, gives the best agreement with these three quantities (Table continued overleaf).

k-point			E(singlet) / eV	E (triplet) / eV	gap / eV	ΔE(singlet) / eV	ΔE (triplet) / eV	Δgap / eV
0.375	0.375	0.375	-6122.006318	-6120.282052	1.724	0.422	0.472	0.050
0.375	0.375	0.125	-6122.046837	-6120.171698	1.875	0.382	0.583	0.201
0.375	0.375	-0.125	-6121.98892	-6120.292181	1.697	0.440	0.462	0.022
0.375	0.375	-0.375	-6121.945992	-6120.341026	1.605	0.483	0.413	0.069
0.375	0.125	0.375	-6121.940838	-6120.163303	1.778	0.488	0.591	0.103
0.375	0.125	0.125	-6121.97528	-6120.071291	1.904	0.453	0.683	0.230
0.375	0.125	-0.125	-6121.925215	-6120.163594	1.762	0.504	0.591	0.087
0.375	0.125	-0.375	-6121.888969	-6120.210859	1.678	0.540	0.544	0.004
0.375	-0.125	0.375	-6121.891634	-6120.144934	1.747	0.537	0.609	0.072

0.375	-0.125	0.125	-6121.933781	-6120.032155	1.902	0.495	0.722	0.227
0.375	-0.125	-0.125	-6121.891197	-6120.113007	1.778	0.538	0.641	0.104
0.375	-0.125	-0.375	-6121.846662	-6120.180143	1.667	0.582	0.574	0.008
0.375	-0.375	0.375	-6121.958404	-6120.261684	1.697	0.470	0.493	0.022
0.375	-0.375	0.125	-6122.00695	-6120.134594	1.872	0.422	0.620	0.198
0.375	-0.375	-0.125	-6121.955386	-6120.245464	1.710	0.473	0.509	0.036
0.375	-0.375	-0.375	-6121.904241	-6120.311249	1.593	0.524	0.443	0.081
0.125	0.375	0.375	-6122.979611	-6121.242383	1.737	-0.551	-0.488	0.063
0.125	0.375	0.125	-6122.931185	-6121.34662	1.585	-0.502	-0.592	0.090
0.125	0.375	-0.125	-6122.886153	-6121.392905	1.493	-0.457	-0.638	0.181
0.125	0.375	-0.375	-6122.938423	-6121.344737	1.594	-0.510	-0.590	0.081
0.125	0.125	0.375	-6122.969357	-6121.244236	1.725	-0.541	-0.490	0.051
0.125	0.125	0.125	-6122.925071	-6121.329941	1.595	-0.496	-0.576	0.079
0.125	0.125	-0.125	-6122.877531	-6121.38282	1.495	-0.449	-0.628	0.180
0.125	0.125	-0.375	-6122.923935	-6121.328774	1.595	-0.495	-0.574	0.079
0.125	-0.125	0.375	-6122.932761	-6121.211798	1.721	-0.504	-0.457	0.047
0.125	-0.125	0.125	-6122.88753	-6121.295426	1.592	-0.459	-0.541	0.082
0.125	-0.125	-0.125	-6122.834415	-6121.349986	1.484	-0.406	-0.596	0.190
0.125	-0.125	-0.375	-6122.882835	-6121.300661	1.582	-0.454	-0.546	0.092
0.125	-0.375	0.375	-6122.943117	-6121.210162	1.733	-0.514	-0.456	0.059
0.125	-0.375	0.125	-6122.892715	-6121.311922	1.581	-0.464	-0.558	0.094
0.125	-0.375	-0.125	-6122.84136	-6121.358585	1.483	-0.413	-0.604	0.192
0.125	-0.375	-0.375	-6122.89583	-6121.314645	1.581	-0.467	-0.560	0.093
0.25	0.375	0.375	-6122.526406	-6120.761538	1.765	-0.098	-0.007	0.091
0.25	0.375	0.125	-6122.516234	-6120.786003	1.730	-0.087	-0.032	0.056
0.25	0.375	-0.125	-6122.446597	-6120.875649	1.571	-0.018	-0.121	0.103
0.25	0.375	-0.375	-6122.456751	-6120.883467	1.573	-0.028	-0.129	0.101
0.25	0.125	0.375	-6122.483413	-6120.707047	1.776	-0.055	0.047	0.102
0.25	0.125	0.125	-6122.478241	-6120.720537	1.758	-0.050	0.034	0.083
0.25	0.125	-0.125	-6122.412	-6120.801428	1.611	0.017	-0.047	0.064
0.25	0.125	-0.375	-6122.417552	-6120.812612	1.605	0.011	-0.058	0.069
0.25	-0.125	0.375	-6122.426385	-6120.672267	1.754	0.002	0.082	0.080
0.25	-0.125	0.125	-6122.425057	-6120.659827	1.765	0.004	0.095	0.091
0.25	-0.125	-0.125	-6122.355328	-6120.753012	1.602	0.073	0.001	0.072
0.25	-0.125	-0.375	-6122.356637	-6120.771805	1.585	0.072	-0.017	0.089
0.25	-0.375	0.375	-6122.468564	-6120.726487	1.742	-0.040	0.028	0.068
0.25	-0.375	0.125	-6122.462493	-6120.725551	1.737	-0.034	0.029	0.063
0.25	-0.375	-0.125	-6122.388481	-6120.827677	1.561	0.040	-0.073	0.114
0.25	-0.375	-0.375	-6122.395458	-6120.840612	1.555	0.033	-0.086	0.119

Table S3. Determination of the mean-value k-point for the monoclinic structure of cocrystal **A:2**. The energies for the singlet, triplet and singlet-triplet gap of the converged k-point grid are -17191.770 eV, -17190.033 eV and 1.738 eV, respectively. The $(-1/4, 1/4, 3/8)$ k-point, shown in red, gives the best agreement with these three quantities.

k-point			E(singlet) / eV	E (triplet) / eV	gap / eV	ΔE(singlet) / eV	ΔE (triplet) / eV	Δgap / eV
-0.375	-0.125	0.375	-17190.94507	-17189.182	1.763	0.825	0.851	0.026
-0.375	0.125	0.125	-17190.94519	-17189.185	1.760	0.825	0.848	0.023
-0.125	-0.375	-0.375	-17192.57765	-17190.822	1.756	-0.807	-0.789	0.018
-0.125	0.375	0.375	-17192.57704	-17190.820	1.757	-0.807	-0.788	0.019
0.125	-0.375	-0.125	-17192.57676	-17190.820	1.757	-0.806	-0.787	0.019
0.125	-0.375	0.125	-17192.57772	-17190.822	1.756	-0.807	-0.789	0.018
0.125	-0.125	-0.375	-17192.15111	-17190.46902	1.682	-0.381	-0.436	0.056
0.125	-0.125	-0.125	-17192.15179	-17190.4672	1.685	-0.381	-0.434	0.053
0.125	-0.125	0.125	-17192.14964	-17190.47251	1.677	-0.379	-0.440	0.061
0.125	-0.125	0.375	-17192.14991	-17190.47526	1.675	-0.379	-0.442	0.063
0.375	-0.375	0.125	-17191.40143	-17189.56462	1.837	0.369	0.468	0.099
0.375	-0.375	0.375	-17191.40219	-17189.56547	1.837	0.368	0.467	0.099
0.375	0.125	0.125	-17190.94613	-17189.1864	1.760	0.824	0.846	0.022
0.375	0.125	0.375	-17190.94545	-17189.18266	1.763	0.825	0.850	0.025
0.375	0.375	-0.375	-17191.4023	-17189.5658	1.837	0.368	0.467	0.099
0.375	0.375	-0.125	-17191.4014	-17189.56482	1.837	0.369	0.468	0.099
0.25	-0.375	-0.375	-17192.00107	-17190.20669	1.794	-0.231	-0.174	0.057
0.25	0.375	0.375	-17192.00174	-17190.20727	1.794	-0.231	-0.175	0.057
0.25	-0.375	-0.125	-17192.00053	-17190.20574	1.795	-0.230	-0.173	0.057
0.25	-0.375	0.125	-17192.00175	-17190.20687	1.795	-0.231	-0.174	0.057
0.25	-0.125	-0.375	-17191.55837	-17189.84304	1.715	0.212	0.190	0.022
0.25	-0.125	-0.125	-17191.55895	-17189.83968	1.719	0.211	0.193	0.018
0.25	-0.125	0.125	-17191.55935	-17189.83623	1.723	0.211	0.197	0.015
0.25	-0.125	0.375	-17191.55867	-17189.83949	1.719	0.212	0.193	0.018
0.25	0.25	0.125	-17191.77941	-17190.02099	1.758	-0.009	0.012	0.021
-0.25	0.25	0.125	-17191.78048	-17190.02414	1.756	-0.010	0.009	0.019
0.25	0.25	0.375	-17191.77964	-17190.02334	1.756	-0.009	0.009	0.019
-0.25	0.25	0.375	-17191.78105	-17190.02684	1.754	-0.011	0.006	0.017

Table S4. Determination of the mean-value k-point for the monoclinic structure of cocrystal **A:3**. The energies for the singlet, triplet and singlet-triplet gap of the converged k-point grid are -17421.031 eV, -17419.245 eV and 1.787 eV, respectively. The $(-1/4, 1/4, 3/8)$ k-point, shown in red, gives the best agreement with these three quantities.

k-point			E(singlet) / eV	E (triplet) / eV	gap / eV	ΔE(singlet) / eV	ΔE (triplet) / eV	Δgap / eV
-0.375	-0.125	0.375	-17420.27153	-17418.471	1.801	0.760	0.774	0.014
-0.375	0.125	0.125	-17420.27129	-17418.474	1.797	0.760	0.770	0.010
-0.125	-0.375	-0.375	-17421.74958	-17419.950	1.800	-0.718	-0.705	0.013
-0.125	0.375	0.375	-17421.74986	-17419.949	1.801	-0.718	-0.704	0.014
0.125	-0.375	-0.125	-17421.75057	-17419.949	1.802	-0.719	-0.704	0.015
0.125	-0.375	0.125	-17421.75103	-17419.951	1.800	-0.720	-0.706	0.013
0.125	-0.125	-0.375	-17421.30412	-17419.568	1.736	-0.273	-0.323	0.050
0.125	-0.125	-0.125	-17421.30376	-17419.565	1.739	-0.272	-0.320	0.048
0.125	-0.125	0.125	-17421.30302	-17419.576	1.727	-0.272	-0.331	0.060
0.125	-0.125	0.375	-17421.30361	-17419.579	1.725	-0.272	-0.334	0.062
0.375	-0.375	0.125	-17420.79559	-17418.928	1.867	0.236	0.316	0.080
0.375	-0.375	0.375	-17420.7961	-17418.929	1.868	0.235	0.316	0.081
0.375	0.125	0.125	-17420.27109	-17418.473	1.798	0.760	0.772	0.011
0.375	0.125	0.375	-17420.27169	-17418.470	1.802	0.760	0.775	0.015
0.375	0.375	-0.375	-17420.7965	-17418.929	1.867	0.235	0.315	0.080
0.375	0.375	-0.125	-17420.79594	-17418.929	1.867	0.235	0.315	0.080
0.25	-0.375	-0.375	-17421.28342	-17419.45226	1.831	-0.252	-0.208	0.044
0.25	0.375	0.375	-17421.28279	-17419.45117	1.832	-0.251	-0.207	0.045
0.25	-0.375	-0.125	-17421.28263	-17419.45047	1.832	-0.251	-0.206	0.045
0.25	-0.375	0.125	-17421.2834	-17419.45078	1.833	-0.252	-0.206	0.046
0.25	-0.125	-0.375	-17420.79741	-17419.03904	1.758	0.234	0.206	0.028
0.25	-0.125	-0.125	-17420.79741	-17419.03195	1.765	0.234	0.213	0.021
0.25	-0.125	0.125	-17420.79794	-17419.02842	1.770	0.233	0.216	0.017
0.25	-0.125	0.375	-17420.79773	-17419.03533	1.762	0.234	0.209	0.024
0.25	0.25	0.125	-17421.04086	-17419.23998	1.801	-0.009	0.005	0.014
-0.25	0.25	0.125	-17421.04139	-17419.2429	1.798	-0.010	0.002	0.012
0.25	0.25	0.375	-17421.04015	-17419.24329	1.797	-0.009	0.001	0.010
-0.25	0.25	0.375	-17421.04034	-17419.24586	1.794	-0.009	-0.001	0.008

Table S5. Determination of the mean-value k-point for the monoclinic structure of cocrystal **A:4**. The energies for the singlet, triplet and singlet-triplet gap of the converged k-point grid are -18749.496 eV, -18747.734 eV and 1.762 eV, respectively. The $(-1/4, 1/4, 3/8)$ k-point, shown in red, gives the best agreement with these three quantities.

	k-point		E(singlet) / eV	E (triplet) / eV	gap / eV	ΔE(singlet) / eV	ΔE (triplet) / eV	Δgap / eV
-0.375	-0.125	0.375	-18748.82185	-18747.04882	1.773	0.674	0.685	0.011
-0.375	0.125	0.125	-18748.82148	-18747.05117	1.770	0.674	0.683	0.009
-0.125	-0.375	-0.375	-18750.12162	-18748.34534	1.776	-0.626	-0.611	0.015
-0.125	0.375	0.375	-18750.12085	-18748.34288	1.778	-0.625	-0.609	0.016
0.125	-0.375	-0.125	-18750.12021	-18748.34146	1.779	-0.624	-0.607	0.017
0.125	-0.375	0.125	-18750.12101	-18748.34395	1.777	-0.625	-0.610	0.015
0.125	-0.125	-0.375	-18749.65664	-18747.93424	1.722	-0.161	-0.200	0.039
0.125	-0.125	-0.125	-18749.65727	-18747.93238	1.725	-0.161	-0.198	0.037
0.125	-0.125	0.125	-18749.65594	-18747.94139	1.715	-0.160	-0.207	0.047
0.125	-0.125	0.375	-18749.65543	-18747.94333	1.712	-0.160	-0.209	0.050
0.375	-0.375	0.125	-18749.37606	-18747.54821	1.828	0.120	0.186	0.066
0.375	-0.375	0.375	-18749.37663	-18747.54808	1.829	0.119	0.186	0.067
0.375	0.125	0.125	-18748.82228	-18747.05167	1.771	0.674	0.683	0.009
0.375	0.125	0.375	-18748.8223	-18747.04897	1.773	0.674	0.685	0.012
0.375	0.375	-0.375	-18749.37746	-18747.54876	1.829	0.118	0.185	0.067
0.375	0.375	-0.125	-18749.37667	-18747.54867	1.828	0.119	0.185	0.066
0.25	-0.375	-0.375	-18749.76455	-18747.96464	1.800	-0.269	-0.230	0.038
0.25	0.375	0.375	-18749.7645	-18747.96357	1.801	-0.269	-0.229	0.039
0.25	-0.375	-0.125	-18749.76392	-18747.96309	1.801	-0.268	-0.229	0.039
0.25	-0.375	0.125	-18749.7641	-18747.96224	1.802	-0.268	-0.228	0.040
0.25	-0.125	-0.375	-18749.25497	-18747.51654	1.738	0.241	0.218	0.023
0.25	-0.125	-0.125	-18749.25562	-18747.51131	1.744	0.240	0.223	0.017
0.25	-0.125	0.125	-18749.25511	-18747.50715	1.748	0.241	0.227	0.014
0.25	-0.125	0.375	-18749.25477	-18747.51273	1.742	0.241	0.221	0.020
0.25	0.25	0.125	-18749.51004	-18747.73495	1.775	-0.014	-0.001	0.013
-0.25	0.25	0.125	-18749.51092	-18747.73827	1.773	-0.015	-0.004	0.011
0.25	0.25	0.375	-18749.50945	-18747.73769	1.772	-0.014	-0.004	0.010
-0.25	0.25	0.375	-18749.50986	-18747.74053	1.769	-0.014	-0.006	0.008

1.2.2 Calculation of the oscillator strengths

Oscillator strengths were calculated for a few lowest excited states using the PBE functional. States having the highest oscillator strengths contribute most to light absorption and, consequently fluorescence emission.

The calculated oscillator strengths for all crystal structures are given in Tables S6-S11. The dominant excited state for the triclinic cells is S_1, while the monoclinic cells showed the highest oscillator strengths for the states S_1 and S_3. The intermediate state S_2, however, has been classified as a spurious state. Spurious states are a known artefact of TD-DFT, they do not correspond to physical electronic excitations.[7] Consequently, the calculated state S_3 corresponds to the experimentally observed state S_2. In order to be certain about the assignment of TD-DFT excited states, additional tests were performed, as described in section 2.2.4.

Table S6. Calculated oscillator strengths for the experimental triclinic structure of cocrystal **A:1**. Excited state S_1 having the largest oscillator strength was used to model the fluorescence spectrum.

Excited state	Excitation energy / eV	Oscillator strength
S_1	2.273	3.7938
S_2	2.622	0.4691
S_3	2.664	0.1401
S_4	3.136	0.0180
S_5	3.235	0.1015

Table S7. Calculated oscillator strengths for the hypothetical monoclinic structure of cocrystal **A:1**. Excited state S_1 and S_3 were used to model the fluorescence spectrum. Note an extremely small oscillator strength for the spurious state S_2.

Excited state	Excitation energy / eV	Oscillator strength
S_1	1.818	0.7113
S_2	1.836	0.0006
S_3	2.155	5.4609
S_4	2.265	0.0098
S_5	2.302	0.5741

Table S8. Calculated oscillator strengths for the hypothetical triclinic structure of cocrystal **A:2**. Excited state S_1 having the largest oscillator strength was used to model the fluorescence spectrum.

Excited state	Excitation energy / eV	Oscillator strength
S_1	2.279	5.3303
S_2	2.619	0.0085
S_3	2.689	0.0146
S_4	2.870	0.0178
S_5	3.131	0.0325

Table S9. Calculated oscillator strengths for the experimental monoclinic structure of cocrystal **A:2**. Excited state S_1 and S_3 were used to model the fluorescence spectrum. Note an extremely small oscillator strength for the spurious state S_2.

Excited state	Excitation energy / eV	Oscillator strength
S_1	1.841	0.3883
S_2	1.852	0.0332
S_3	2.203	9.1854
S_4	2.457	0.0674
S_5	2.467	0.0016

Table S10. Calculated oscillator strengths for the hypothetical triclinic structure of cocrystal **A:3**. Excited state S_1 having the largest oscillator strength was used to model the fluorescence spectrum.

Excited state	Excitation energy / eV	Oscillator strength
S_1	2.325	5.1400
S_2	2.652	0.0362
S_3	2.927	0.0048
S_4	3.003	0.0155
S_5	3.141	0.0268

Table S11. Calculated oscillator strengths for the experimental monoclinic structure of cocrystal **A:3**. Excited state S_1 and S_3 were used to model the fluorescence spectrum. Note an extremely small oscillator strength for the spurious state S_2.

Excited state	Excitation energy / eV	Oscillator strength
S_1	1.887	0.4843
S_2	1.900	0.0111
S_3	2.251	9.3012
S_4	2.515	0.0063
S_5	2.522	0.0173

Table S12. Calculated oscillator strengths for the hypothetical triclinic structure of cocrystal **A:4**. Excited state S_1 having the largest oscillator strength was used to model the fluorescence spectrum.

Excited state	Excitation energy / eV	Oscillator strength
S_1	2.262	4.857
S_2	2.444	0.0105
S_3	2.645	0.3768
S_4	2.978	0.0106
S_5	3.192	0.0192

Table S13. Calculated oscillator strengths for the experimental monoclinic structure of cocrystal **A:4**. Excited state S_1 and S_3 were used to model the fluorescence spectrum. Note an extremely small oscillator strength for the spurious state S_2.

Excited state	Excitation energy / eV	Oscillator strength
S_1	1.859	0.4023
S_2	1.868	0.0005
S_3	2.211	9.4627
S_4	2.387	0.0167
S_5	2.395	0.0264

1.2.3 TD-DFT geometry optimization

TD-DFT geometry optimization was performed for the states selected based on their oscillator strengths (S_1 for the triclinic structures, S_1 and S_3 for the monoclinic structures).

Optimization of the excited states was performed using the PBE functional with the mean-value k-point. The following convergence criteria were used: energy tolerance 10^{-5} eV/atom, maximum atomic force $3x10^{-2}$ eV $Å^{-1}$, maximum atom displacement 10^{-3} Å. The cell parameters were kept fixed at the values derived from the ground state geometry optimization.

1.2.4 Analysis of spurious states – the role of exact exchange

In order to model the fluorescence spectra correctly it is necessary to rule out any unphysical electronic excitations. It has been found that increasing the contribution of exact exchange in DFT functionals improves the accuracy of the excitation energies and provide a better description for Charge Transfer (CT) states.[8,9] Nonetheless, even when hybrid functionals are used, there is a risk of finding CT states among the low-lying excited states. TD-DFT can be compared with the time-dependent Hartree-Fock method (TD-HF), where the latter improves the description of CT excitations. The ordering of the excitations remains the same between the two methods, hence we conclude that CT excitations are not dominant (which is more likely than CT excitations are present and incorrectly described in TD-DFT to the same degree in all crystals studied).We find that the excitation energies determined by TD-HF, however, are usually overestimated.

In the present work single-point TD-DFT calculations were performed using a hybrid B3LYP functional to improve the accuracy over the original PBE calculations. In addition, single-point TD-DFT calculations were performed in order to ensure that the excited states under consideration are the true electronic excitations and not the artefact of TD-DFT. The comparison of PBE, B3LYP and HF calculations is given in Tables S14-S21.

Perhaps the reader may ask why could hybrid functionals not be used throughout the calculation process. There are two reasons for this:

1) Current implementation of TD-DFT in CASTEP allows to perform hybrid calculations only at the gamma k-point. We have seen, however, that using the mean-value k-point gives a great improvement in the accuracy of fluorescence calculations.
2) Calculation of HF exchange is extremely expensive in the plane-wave formalism. By performing the geometry optimization using the semi-local PBE functionals and correcting the final excitation energies with the hybrid calculations we have saved 1000s of CPU hours of computer time.

To conclude, we believe that the decision to use PBE functional for geometry optimization followed by B3LYP single-point calculations has given us the best balance of accuracy and performance at present. Depending on the development of periodic TD-DFT and the available computer power, full hybrid calculations may become practical in the future.

Table S14. TD-DFT and TD-HF band transitions for the experimentally found triclinic structure of **A:1** cocrystal. Excited states S1-S5 are shown, transitions contributing less than 10% to the electronic excitation were omitted. B3LYP functional was used to calculate the emission spectrum. PBE0 was used for comparison. Evidently, the results of both hybrid functionals (B3LYP and PBE0) are very similar.

Excited state	Mean-value k-point	Gamma k-point			
	PBE	PBE	B3LYP	PBE0	HF
S_1	2.273 eV 82-->83 0.9126	1.980 eV 82-->83 0.9633	2.204 eV 82-->83 0.9817	2.284 eV 82-->83 0.9822	2.984 eV 82-->83 0.8960
S_2	2.622 eV 81-->83 0.5433 80-->83 0.4166	2.5474 eV 82-->84 0.7216 80-->83 0.2716	2.992 eV 82-->84 0.7999 80-->83 0.1903	3.121 eV 82-->84 0.8128 80-->83 0.1756	4.391 eV 82-->84 0.6961 80-->83 0.1513
S_3	2.664 eV 82-->84 0.4976 80-->83 0.3080	2.548 eV 81-->83 0.9965	3.162 eV 81-->83 0.9946	3.280 eV 81-->83 0.9929	5.126 eV 79-->83 0.4127 82-->87 0.1518
S_4	3.136 eV 79-->83 0.7855 78-->83 0.1713	3.131 eV 79-->83 0.7545 78-->83 0.1735	3.684 eV 79-->83 0.6579 82-->86 0.2971	3.815 eV 79-->83 0.6199 82-->86 0.3115	5.252 eV 82-->85 0.3490 78-->84 0.1239 76-->83 0.1057 80-->83 0.1051
S_5	3.235 eV 81-->84 0.2716 82-->85 0.2035 82-->84 0.1282	3.219 eV 82-->86 0.7324 78 -->83 0.2367	3.749 eV 82-->85 0.8767	3.882 eV 82-->85 0.8167	5.420 eV 78-->83 0.2649 76-->84 0.1480 77-->83 0.1296

Table S15. TD-DFT and TD-HF band transitions for the hypothetical monoclinic structure of **A:1** cocrystal. Excited states S1-S5 are shown, transitions contributing less than 10% to the electronic excitation were omitted, except for TD-HF S_5 state where none of the transitions contributed 10%.

Excited state	Mean-value k-point	Gamma k-point			
	PBE	PBE	B3LYP	PBE0	HF
S_1	1.818 eV 164-->165 0.7161 163-->166 0.2714	1.672 eV 164-->165 0.7480 163-->166 0.2498	2.477 eV 164-->165 0.6637 163-->166 0.2758	2.600 eV 164-->165 0.6040 163-->166 0.3221	3.424 eV 164-->165 0.3723 163-->166 0.3396
S_2	1.836 eV 163-->165 0.4980	1.678 eV 164-->166 0.5054	2.908 eV 162-->165 0.2789	3.034 eV 162-->165 0.2449	3.921 eV 163-->165 0.3307

	164-->166 0.4972	163-->165 0.4943	164-->166 0.2420 161-->166 0.2309 163-->165 0.1755	164-->166 0.2372 163-->165 0.2163 161-->166 0.2100	164-->166 0.3191
S_3	2.155 eV 163-->166 0.6120 164-->165 0.2187	2.041 eV 163-->166 0.6566 164-->165 0.2018	2.986 eV 163-->165 0.5308 164-->166 0.3893	3.229 eV 161-->165 0.4959 162-->166 0.4281	4.694 eV 159-->165 0.2134 160-->166 0.1896 163-->167 0.1838 164-->168 0.1523
S_4	2.265 eV 162-->165 0.5280 161-->165 0.2890	2.186 eV 162-->165 0.6369 161-->166 0.1202 164-->166 0.1175 163-->165 0.1134	3.012 eV 163-->166 0.6558 164-->165 0.2677	3.296 eV 163-->165 0.5247 164-->166 0.3385	4.925 eV 160-->165 0.2087 164-->167 0.1811 159-->166 0.1628 163-->168 0.1238
S_5	2.301 eV 161-->165 0.3799 162-->165 0.3012 162-->166 0.2300	2.291 eV 161-->165 0.7314 162-->166 0.2431	3.087 eV 161-->165 0.5180 162-->166 0.4251	3.321 eV 163-->166 0.5682 164-->165 0.3011	5.362 eV 158-->165 0.0796 157-->166 0.0795 158-->166 0.0712 157-->165 0.0709

Table S16. TD-DFT and TD-HF band transitions for the hypothetical triclinic structure of **A:2** cocrystal. Excited states S1-S4 are shown, transitions contributing less than 10% to the electronic excitation were omitted.

Excited state	Mean-value k-point	Gamma k-point			
	PBE	PBE	B3LYP	PBE0	HF
S_1	2.272 eV 94 -->95 0.9542	2.222 eV 94-->95 0.9612	2.457 eV 94-->95 0.9805	2.540 eV 94-->95 0.9808	3.230 eV 94-->95 0.8785
S_2	2.619 eV 94-->96 0.5451 93-->95 0.4514	2.650 eV 93-->95 0.9967	3.126 eV 94-->96 0.7631 92-->95 0.2277	3.253 eV 94-->96 0.7803 92-->95 0.2089	4.479 eV 94-->96 0.6873 93-->95 0.1638
S_3	2.689 eV 92-->95 0.9913	2.678 eV 94-->96 0.6820 91-->95 0.3118	3.397 eV 93-->95 0.9945	3.502 eV 93-->95 0.9937	5.298 eV 91-->95 0.4055
S_4	2.870 eV 91-->95 0.9964	2.800 eV 92-->95 0.9974	3.581 eV 94-->97 0.9957	3.767 eV 94-->97 0.9918	5.380 eV 94-->99 0.1909 87-->95 0.1611 94-->98 0.1454
S_5	2.870 eV 94-->97 0.9659	2.870 eV 94-->97 0.9891	3.673 eV 94-->98 0.9782	3.673 eV 91-->95 0.9891	5.497 eV 89-->95 0.2276 87-->96 0.1962 94-->104 0.1213 90-->95 0.1092

Table S17. TD-DFT and TD-HF band transitions for the experimentally found monoclinic structure of **A:2** cocrystal. Excited states S1-S4 are shown, transitions contributing less than 10% to the electronic excitation were omitted.

Excited state	Mean-value k-point	Gamma k-point			
	PBE	PBE	B3LYP	PBE0	HF
S_1	1.841 eV 188-->189 0.6385 187-->190 0.3024	1.728 eV 188-->189 0.7305 187-->190 0.2681	2.512 eV 188-->189 0.7295 187-->190 0.2246	2.638 eV 188-->189 0.6524 187-->190 0.2883	3.433 eV 188-->189 0.3841 187-->190 0.3366
S_2	1.852 eV 188-->190 0.4783 187-->189 0.4606	1.750 eV 188-->190 0.5080 187-->189 0.4919	2.895 eV 188-->190 0.4928 187-->189 0.4389	3.181 eV 188-->190 0.5377 187-->189 0.3518	3.914 eV 187-->189 0.3323 188-->190 0.3285
S_3	2.203 eV 187-->190 0.6326 188-->189 0.3104	2.128 eV 187-->190 0.7002 188-->189 0.2478	2.930 eV 187-->190 0.7200 188-->189 0.2152	3.208 eV 187-->190 0.6296 188-->189 0.2662	4.631 eV 186-->190 0.2077 185-->189 0.1965 188-->192 0.1778 187-->191 0.1711
S_4	2.457 eV 188-->191 0.5895 186-->189 0.2624 187-->192 0.1117	2.451 eV 188-->192 0.7162 187-->191 0.2442	3.126 eV 187-->189 0.4184 188-->190 0.3599	3.126 eV 187-->189 0.4883 188-->190 0.2930	4.913 eV 186-->189 0.2063 188-->191 0.1861 185-->190 0.1639 187-->192 0.1271
S_5	2.467 eV 188-->192 0.6509 187-->191 0.2103	2.453 eV 186-->189 0.5543 188-->191 0.1233	3.404 eV 188-->192 0.4648 187-->191 0.2010 185-->189 0.1374 186-->190 0.1293	3.497 eV 184-->189 0.5086 185-->190 0.4188	5.347 eV 182-->190 0.1537 181-->189 0.1527

Table S18. TD-DFT and TD-HF band transitions for the hypothetical triclinic structure of **A:3** cocrystal. Excited states S1-S4 are shown, transitions contributing less than 10% to the electronic excitation were omitted.

Excited state	Mean-value k-point	Gamma k-point			
	PBE	PBE	B3LYP	PBE0	HF
S_1	2.325 eV 94-->95 0.9533	2.217 eV 94-->95 0.9623	2.453 eV 94-->95 0.9812	2.538 eV 94-->95 0.9817	3.242 eV 94-->95 0.8813 93-->96 0.0595
S_2	2.652 eV 94-->96 0.5382 93-->95 0.4578	2.702 eV 94-->96 0.6658 91-->95 0.3290	3.162 eV 94-->96 0.7422 93-->95 0.2500	3.293 eV 94-->96 0.7567 93-->95 0.2342	4-562 eV 94-->96 0.6735 93-->95 0.1717
S_3	2.927 eV 92-->95 0.9978	2.831 eV 93-->95 0.9975	3.577 eV 94-->97 0.9969	3.776 eV 94-->97 0.9926	5.330 eV 91-->95 0.3891 94-->102 0.1286 94-->101 0.1085 92-->95 0.1051
S_4	3.003 eV 91-->95 0.9936	2.901 eV 92-->95 0.9974	3.667 eV 92-->95 0.9933	3.790 eV 92-->95 0.9953	5.408 eV 94-->99 0.2243 88-->95 0.1896 90-->96 0.1194
S_5	3.141 eV 94-->97 0.9870	3.041 eV 94-->97 0.9974	3.688 eV 94-->98 0.9768	3.876 eV 94-->98 0.9574	5.525 eV 90-->95 0.2758 88-->96 0.2052 94-->103 0.1315

Table S19. TD-DFT and TD-HF band transitions for the experimentally found monoclinic structure of **A:3** cocrystal. Excited states S1-S4 are shown, transitions contributing less than 10% to the electronic excitation were omitted, except for TD-HF S_5 state where none of the transitions contributed 10%.

Excited state	Mean-value k-point	Gamma k-point			
	PBE	PBE	B3LYP	PBE0	HF
S_1	1.887 eV 188-->189 0.6685 187-->190 0.3082	1.788 eV 188-->189 0.7560 187-->190 0.2423	2.565 eV 188-->189 0.7713 187-->190 0.1841	2.697 eV 188-->189 0.6894 187-->190 0.2526	3.505 eV 188-->189 0.3907 187-->190 0.3284
S_2	1.900 eV 188-->190 0.5009 187-->189 0.4790	1.817 eV 188-->190 0.5148 187-->189 0.4850	2.931 eV 188-->190 0.5360 187-->189 0.3928	3.208 eV 188-->190 0.5766 187-->189 0.3106	4.018 eV 188-->190 0.3343 187-->189 0.3251
S_3	2.251 eV 187-->190 0.6548 188-->189 0.3026	2.200 eV 187-->190 0.7346 188-->189 0.2269	2.982 eV 187-->190 0.7587 188-->189 0.1744	3.249 eV 187-->190 0.6621 188-->189 0.2306	4.688 eV 186-->190 0.2190 188-->191 0.1950 185-->189 0.1778 187-->192 0.1587
S_4	2.515 eV 188-->191 0.6758 187-->192 0.2274	2.501 eV 188-->191 0.7837 187-->192 0.1560	3.429 eV 188-->191 0.4822 187-->192 0.1775 186-->190 0.1455 185-->189 0.1382	3.367 eV 187-->189 0.5491 188-->190 0.2850	5.002 eV 186-->189 0.2026 188-->192 0.1942 185-->190 0.1576 187-->191 0.1244
S_5	2.522 eV 188-->192 0.6648 187-->191 0.2884	2.525 eV 188-->192 0.6949 187-->191 0.2258	3.449 eV 188-->192 0.3407 187-->191 0.2995 186-->189 0.1656 185-->190 0.1358	3.655 eV 188-->191 0.1904 188-->192 0.1811 187-->191 0.1516 186-->189 0.1011	5.420 eV 184-->189 0.0823 183-->190 0.0724 188-->205 0.0608 180-->189 0.0573

Table S20. TD-DFT and TD-HF band transitions for the hypothetical triclinic structure of **A:4** cocrystal. Excited states S1-S4 are shown, transitions contributing less than 10% to the electronic excitation were omitted.

Excited state	Mean-value k-point	Gamma k-point			
	PBE	PBE	B3LYP	PBE0	HF
S_1	2.262 eV 99-->100 0.9400	2.169 eV 99-->100 0.9538	2.408 eV 99-->100 0.9802	2.493 eV 99-->100 0.9811	3.208 eV 99-->100 0.8767 98-->101 0.0307 98-->102 0.0268
S_2	2.444 eV 99-->101 0.9824	2.433 eV 99-->101 0.8899 99-->102 0.1052	2.867 eV 99-->101 0.9623	3.088 eV 99-->101 0.8397 99-->102 0.1506	4.577 eV 99-->101 0.4025 99-->102 0.2472 98-->100 0.1909
S_3	2.645 eV 99-->102 0.5466 98-->100 0.4271	2.701 eV 99-->102 0.5871 97-->100 0.3284	3.155 eV 99-->102 0.7038 98-->100 0.2713	3.287 eV 99-->102 0.6486 98-->100 0.2530	5.195 eV 99-->102 0.4520 99-->101 0.3902
S_4	2.978 eV 97-->100 0.9824	2.821 eV 98-->100 0.9686	3.733 eV 97-->100 0.9615	3.827 eV 97-->100 0.9648	5.313 eV 97-->100 0.4593
S_5	3.193 eV 98-->101 0.9675	3.086 eV 96-->100 0.9290	3.905 eV 96-->100 0.4427 99-->103 0.3652	4.039 eV 96-->100 0.6362	5.405 eV 99-->103 0.1809 98-->100 0.1280

Table S21. TD-DFT and TD-HF band transitions for the experimentally found monoclinic structure of **A:4** cocrystal. Excited states S1-S4 are shown, transitions contributing less than 10% to the electronic excitation were omitted.

Excited state	Mean-value k-point	Gamma k-point			
	PBE	PBE	B3LYP	PBE0	HF
S_1	1.859 eV 198-->199 0.6586 197-->200 0.3367	1.776 eV 198-->199 0.7493 197-->200 0.2489	2.567 eV 198-->199 0.7504 197-->200 0.1994	2.702 eV 198-->199 0.6720 197-->200 0.2639	3.530 eV 198-->199 0.3818 197-->200 0.3229
S_2	1.868 eV 197-->199 0.5007 198-->200 0.4982	1.803 eV 198-->200 0.5017 197-->199 0.4980	2.949 eV 198-->200 0.4519 197-->199 0.4267	3.222 eV 197-->199 0.2977 198-->203 0.2346 198-->200 0.1973 197-->204 0.1780	4.049 eV 198-->200 0.3213 197-->199 0.3208
S_3	2.211 eV 197-->200 0.6312 198-->199 0.3153	2.178 eV 197-->200 0.7273 198-->199 0.2332	2.994 eV 197-->200 0.6983 198-->199 0.1671	3.242 eV 198-->204 0.4230 197-->203 0.3917	4.707 eV 196-->200 0.2107 195-->199 0.1840 198-->202 0.1835 197-->201 0.1631
S_4	2.387 eV 198-->201 0.7498 197-->201 0.1565	2.4658 eV 198-->202 0.6970 198-->204 0.1597 197-->201 0.1114	3.018 eV 198-->203 0.3561 197-->204 0.2352 197-->201 0.1839 198-->202 0.1362	3.253 eV 198-->200 0.3272 198-->203 0.2524 197-->204 0.2377	5.010 eV 196-->199 0.2017 198-->201 0.1900 195-->200 0.1514 197-->202 0.1182
S_5	2.395 eV 198-->202 0.7501 197-->202 0.1252	2.4664 eV 198-->201 0.6083 198-->203 0.2283 197-->202 0.1360	3.023 eV 197-->203 0.2962 198-->204 0.2813 198-->201 0.2201 197-->202 0.1110	3.273 eV 197-->200 0.5413 198-->199 0.2141	5.206 eV 197-->204 0.2386 198-->203 0.2378

Table S22. Correspondence between the TD-DFT excited states at the mean-value and gamma k-points.

Crystal structure	Excited states			
	Mean-value k-point	Gamma k-point		
	PBE	PBE	B3LYP	PBE0
A:1 triclinic	S_1	S_1	S_1	S_1
A:1 monoclinic	S_1 S_3	S_1 S_3	S_1 S_4	S_1 S_5
A:2 triclinic	S_1	S_1	S_1	S_1
A:2 monoclinic	S_1 S_3	S_1 S_3	S_1 S_3	S_1 S_3
A:3 triclinic	S_1	S_1	S_1	S_1
A:3 monoclinic	S_1 S_3	S_1 S_3	S_1 S_3	S_1 S_3
A:4 triclinic	S_1	S_1	S_1	S_1
A:4 monoclinic	S_1 S_3	S_1 S_3	S_1 S_3	S_1 S_5

1.2.5 Modelling of fluorescence line shapes

Hybrid functionals, such as B3LYP, provide most accurate excitation energies in TD-DFT calculations. Unfortunately, B3LYP calculations can only be performed at the gamma k-point. In order to approximate the energy difference between these k-points we have performed TD-DFT calculations with PBE functional:

$$\Delta E_{mean-\Gamma} = E_{PBE,mean} - E_{PBE,\Gamma} \quad 1)$$

The energy difference from eq. 1 was used to approximate the B3LYP energy at the mean-value k-point:

$$E_{B3LYP,mean} = E_{B3LYP,\Gamma} + E_{PBE,mean} - E_{PBE,\Gamma} \quad (2)$$

The expression from eq. 2 was used to evaluate the excitation energy corresponding to the optimized geometry of the excited state (E_{max}) the geometry of the ground state (E_0). The lines of the fluorescence spectra were described by a Gaussian function with the maximum at E_{max} and half-width related to the difference between E_{max} and E_0:

$$\sigma = \frac{E_0 - E_{max}}{3} \quad 3)$$

which gives the following expression for the fluorescence intensity:

$$I(E) = e^{-\frac{9}{2}\left(\frac{E-E_{max}}{E_0-E_{max}}\right)^2} \quad 4)$$

Figure S2. Relationship between potential energy surfaces of the ground and excited electronic states (left) and the fluorescence line shape (right).

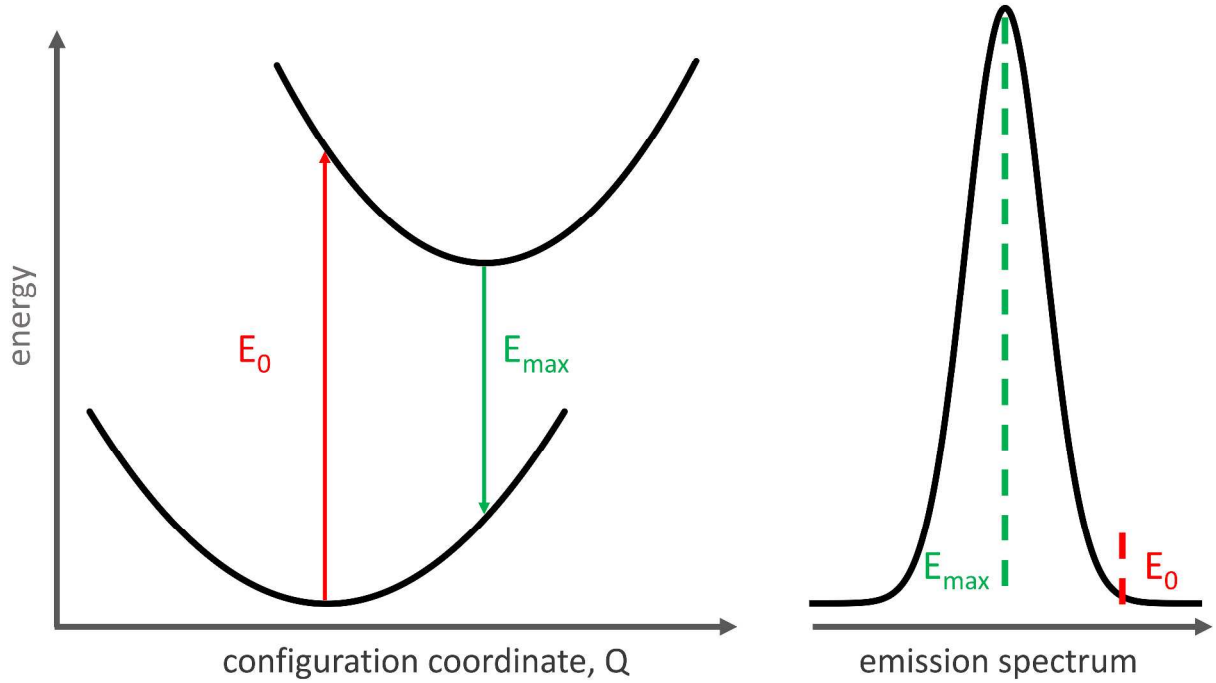

The relationship between potential energy surfaces of the electronic states and the resulting fluorescence line shapes is shown on Figure S2. The quantitative data used to construct fluorescence spectra is given in Tables S23-30.

The approach we have used herein to derive fluorescence line shapes is empirical. A full ab-initio line shape determination would involve phonon calculation both for the ground and excited state. Since TD-DFT calculations are currently restricted to a single k-point, phonon calculation for the electronic excited state would suffer from Brillouin zone convergence issues. Under such circumstances analytical derivation of fluorescence line shapes was deemed unfeasible. The empirical Gaussian line shapes, as we shall see, provide a good approximation to the experimental line shapes at a low computational cost.

Table S23 TD-DFT excitation energies used to model fluorescence spectrum of the **A:1** cocrystal in the triclinic form.

Excited state	Geometry	Energy / eV			
		PBE, mean-value	PBE, Gamma	B3LYP, Gamma	B3LYP, mean-value (derived using eq. 2)
S_1	Ground state	2.2729	1.9802	2.3739	2.6665
	Optimized excited state	2.1120	1.8008	1.9684	2.2797

Table S24. TD-DFT excitation energies used to model fluorescence spectrum of the **A:1** cocrystal in the monoclinic form.

Excited state	Geometry	Energy / eV			
		PBE, mean-value	PBE, Gamma	B3LYP, Gamma	B3LYP, mean-value (derived using eq. 2)
S_1	Ground state	1.8181	1.6720	2.4772	2.6233
	Optimized excited state	1.6453	1.5018	2.2699	2.4134
S_3	Ground state	2.1551	2.0411	3.0128	3.1268
	Optimized excited state	2.0617	1.9498	2.8467	2.9586

Table S25. TD-DFT excitation energies used to model fluorescence spectrum of the **A:2** cocrystal in the triclinic form.

Excited state	Geometry	Energy / eV			
		PBE, mean-value	PBE, Gamma	B3LYP, Gamma	B3LYP, mean-value (derived using eq. 2)
S_1	Ground state	2.2793	2.2222	2.4566	2.5136
	Optimized excited state	2.0848	2.0522	2.2208	2.2533

Table S26. TD-DFT excitation energies used to model fluorescence spectrum of the **A:2** cocrystal in the monoclinic form.

Excited state	Geometry	Energy / eV			
		PBE, mean-value	PBE, Gamma	B3LYP, Gamma	B3LYP, mean-value (derived using eq. 2)
S_1	Ground state	1.8410	1.7283	2.5123	2.6250
	Optimized excited state	1.6598	1.5474	2.2925	2.4049
S_3	Ground state	2.2033	2.1283	2.9300	3.0050
	Optimized excited state	2.1042	2.0313	2.7486	2.8216

Table S27. TD-DFT excitation energies used to model fluorescence spectrum of the **A:3** cocrystal in the triclinic form.

Excited state	Geometry	Energy / eV			
		PBE, mean-value	PBE, Gamma	B3LYP, Gamma	B3LYP, mean-value (derived using eq. 2)
S_1	Ground state	2.3251	2.2168	2.4533	2.5616
	Optimized excited state	2.1400	2.0324	2.2033	2.3108

Table S28. TD-DFT excitation energies used to model fluorescence spectrum of the **A:3** cocrystal in the monoclinic form.

Excited state	Geometry	Energy / eV			
		PBE, mean-value	PBE, Gamma	B3LYP, Gamma	B3LYP, mean-value (derived using eq. 2)
S_1	Ground state	1.8865	1.7880	2.5647	2.6633
	Optimized excited state	1.6923	1.5915	2.3232	2.4240
S_3	Ground state	2.2509	2.2002	2.9817	3.0325
	Optimized excited state	2.1522	2.1038	2.8113	2.8597

Table S29. TD-DFT excitation energies used to model fluorescence spectrum of the **A:4** cocrystal in the triclinic form.

Excited state	Geometry	Energy / eV			
		PBE, mean-value	PBE, Gamma	B3LYP, Gamma	B3LYP, mean-value (derived using eq. 2)
S_1	Ground state	2.2621	2.1695	2.4079	2.5005
	Optimized excited state	2.0716	1.9903	2.1693	2.2506

Table S30. TD-DFT excitation energies used to model fluorescence spectrum of the **A:4** cocrystal in the monoclinic form.

Excited state	Geometry	Energy / eV			
		PBE, mean-value	PBE, Gamma	B3LYP, Gamma	B3LYP, mean-value (derived using eq. 2)
S_1	Ground state	1.8585	1.7762	2.5674	2.6497
	Optimized excited state	1.6638	1.5777	2.3225	2.4085
S_3	Ground state	2.2109	2.1781	2.9941	3.0268
	Optimized excited state	2.0945	2.0639	2.7880	2.8186

1.3 DOS calculations

Density of States (DOS) and Projected Density of States (PDOS) plots were computed for all materials using the program OptaDOS.[10,11] PDOS partitioning was used to evaluate the contribution of coformer molecules to the bands responsible for electronic excitations. DOS were sampled at 0.001 eV intervals and the adaptive broadening[12] scheme was used with the

smearing parameter set to 1 Å. Convergence of the calculated band gap with respect to Brillouin zone sampling was tested and the k-point spacing of 0.015 $Å^{-1}$ was found to be sufficient.

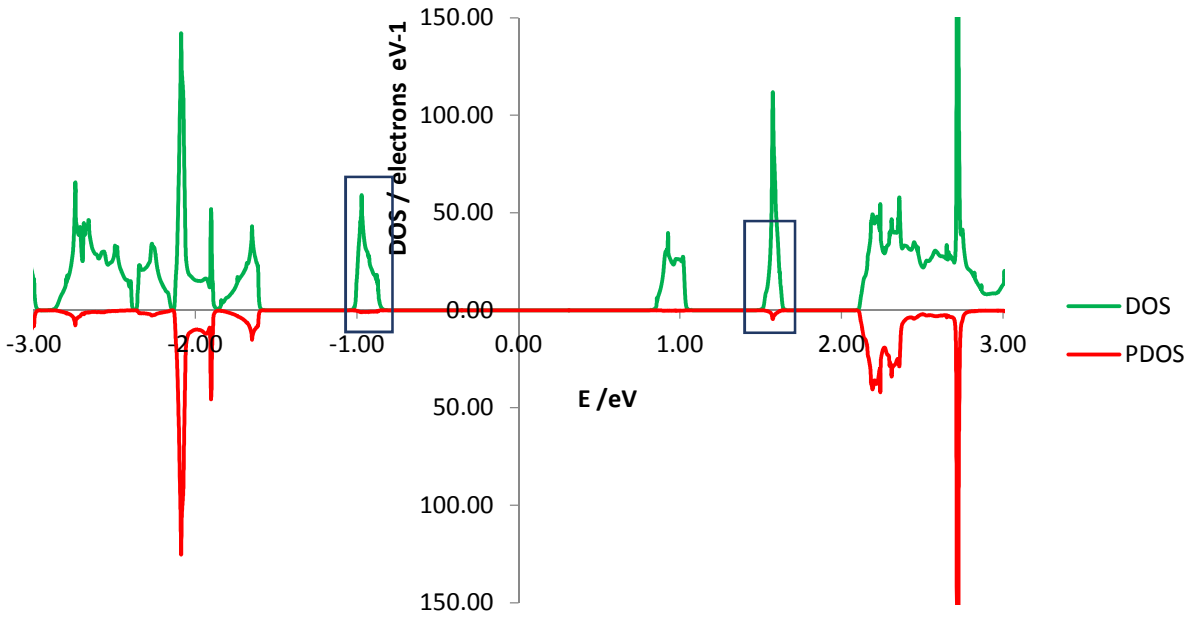

Figure S3. DOS (green) and PDOS (red) plots for the triclinic structure of **A:1** cocrystal. The PDOS plot shows the contribution of coformer molecule to the total DOS. The HOCO (82) and LUCO (83) bands are marked with blue rectangles. It is evident that these bands are almost entirely localized on molecules **A.**

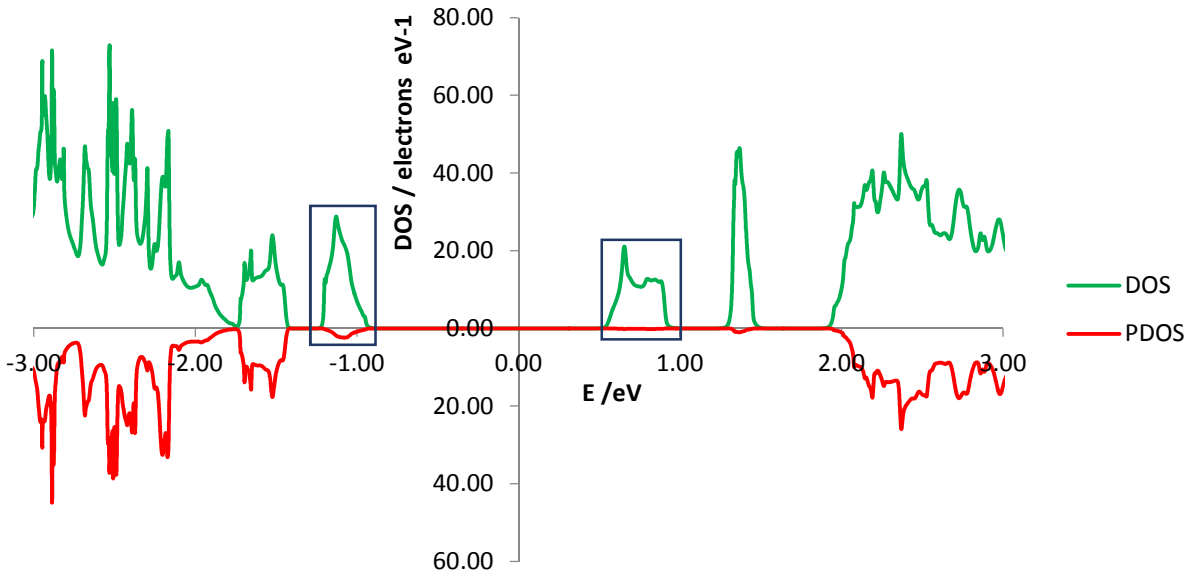

Figure S4. DOS (green) and PDOS (red) plots for the monoclinic structure of **A:1** cocrystal. The PDOS plot shows the contribution of coformer molecule to the total DOS. The pairs of nearly degenerate HOCO (163, 164) and LUCO (165, 166) bands are marked with blue rectangles. It is evident that these bands are almost entirely localized on molecules **A.**

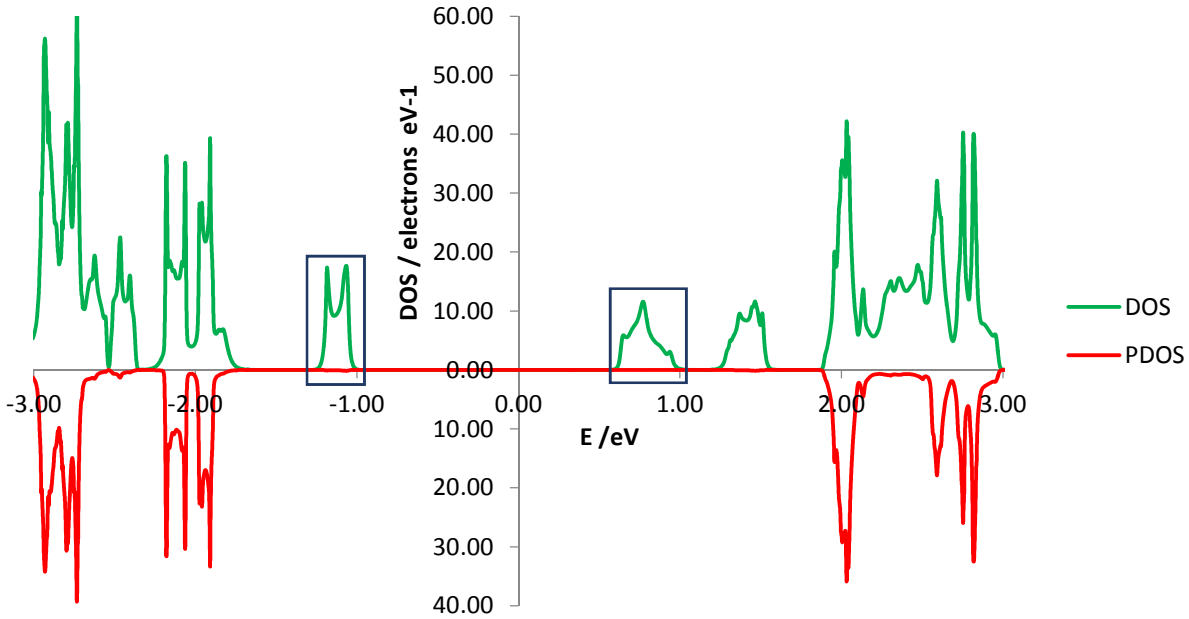

Figure S5. DOS (green) and PDOS (red) plots for the triclinic **A:2** cocrystal. The PDOS plot shows the contribution of coformer molecule to the total DOS.The HOCO (94) and LUCO (95) bands are marked with blue rectangles. It is evident that these bands are almost entirely localized on molecules **A.**

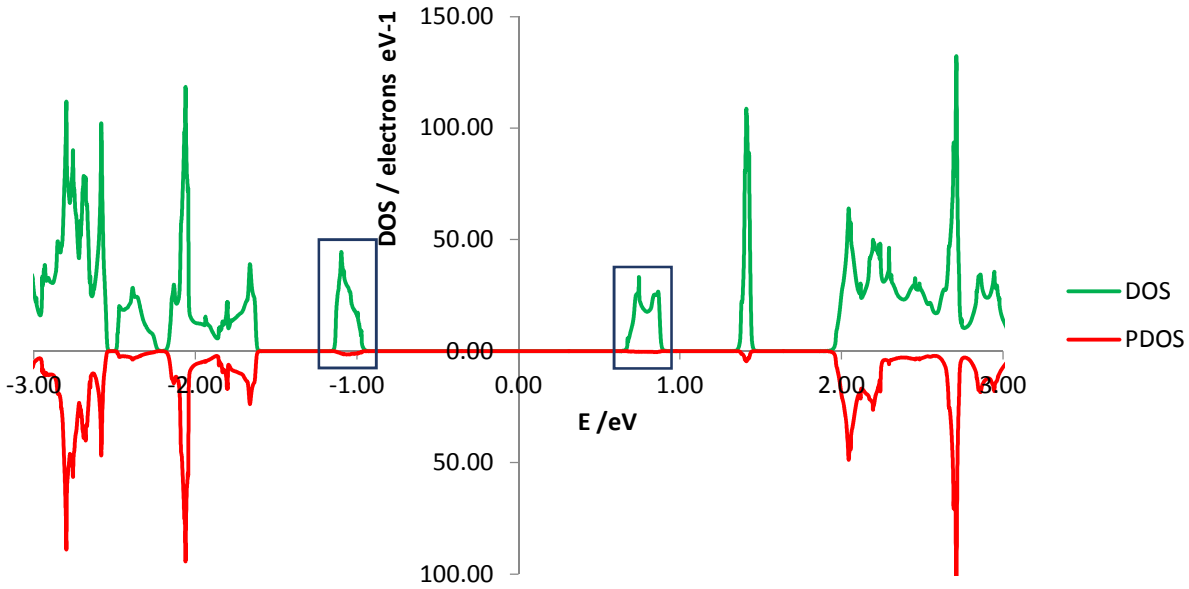

Figure S6. DOS (green) and PDOS (red) plots for the monoclinic structure of **A:2** cocrystal. The PDOS plot shows the contribution of coformer molecule to the total DOS. The pairs of nearly degenerate HOCO (187, 188) and LUCO (189, 190) bands are marked with blue rectangles. It is evident that these bands are almost entirely localized on molecules **A.**

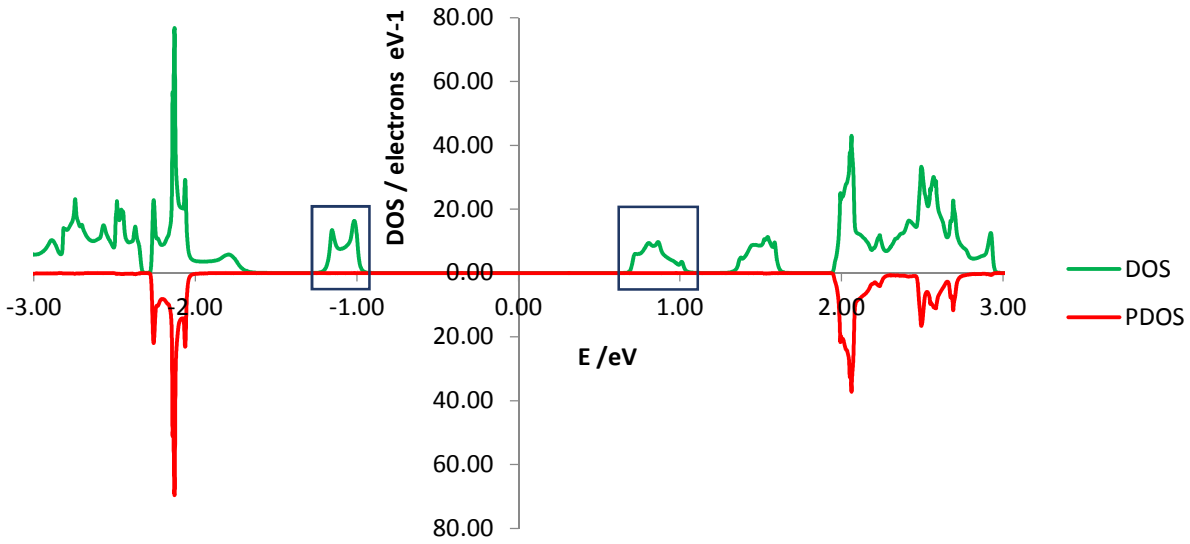

Figure S7. DOS (green) and PDOS (red) plots for the triclinic **A:3** cocrystal. The PDOS plot shows the contribution of coformer molecule to the total DOS. The HOCO (94) and LUCO (95) bands are marked with blue rectangles. It is evident that these bands are almost entirely localized on molecules **A.**

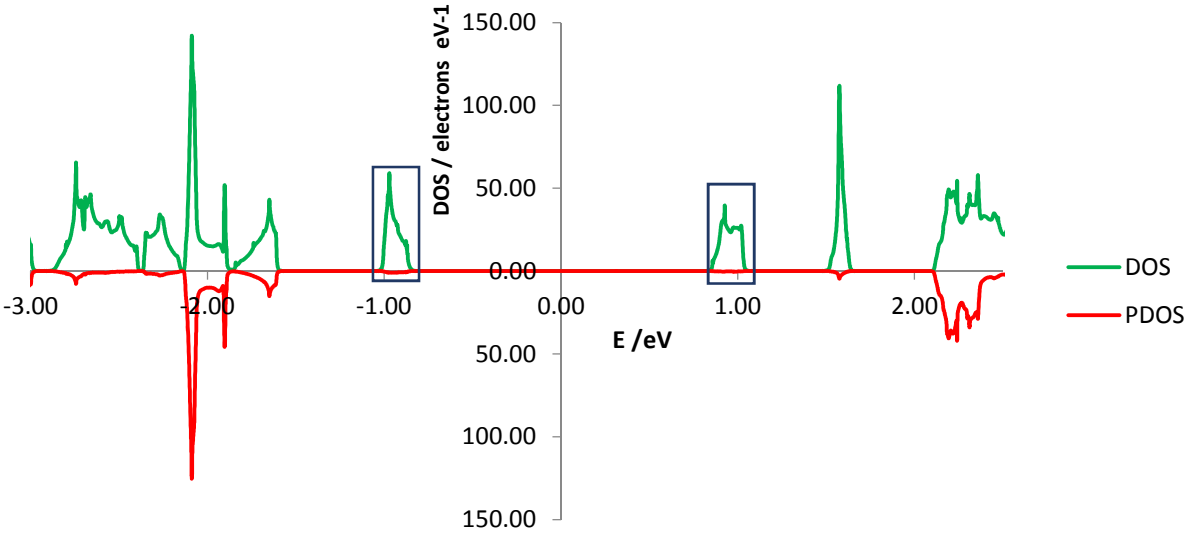

Figure S8. DOS (green) and PDOS (red) plots for the monoclinic structure of **A:3** cocrystal. The PDOS plot shows the contribution of coformer molecule to the total DOS. The pairs of nearly degenerate HOCO (187, 188) and LUCO (189, 190) bands are marked with blue rectangles. It is evident that these bands are almost entirely localized on molecules **A.**

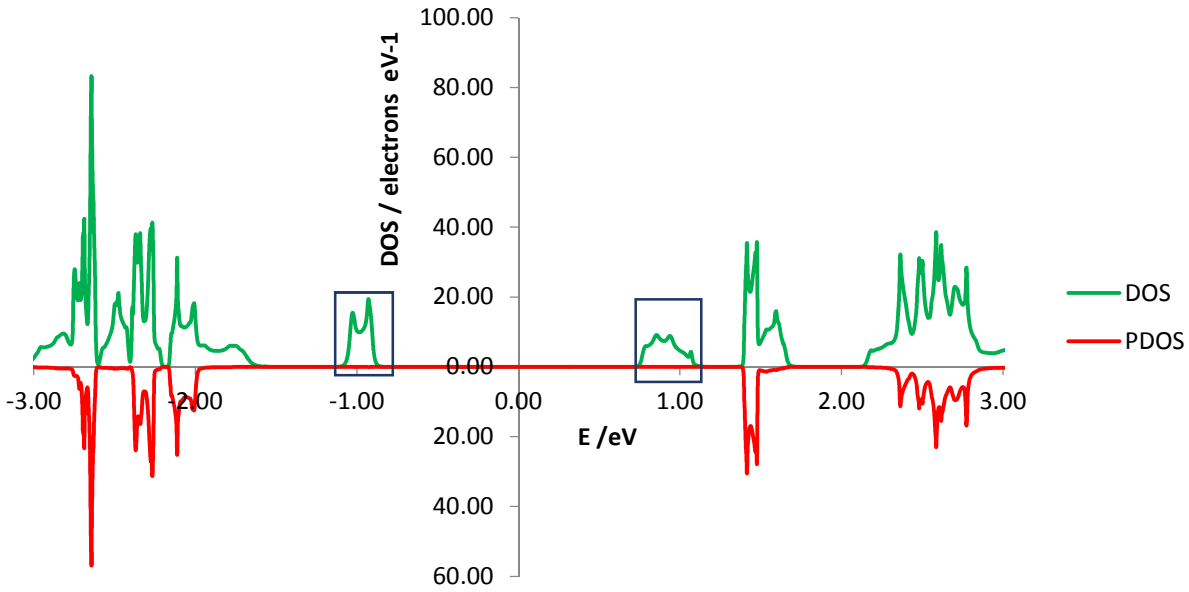

Figure S9. DOS (green)and PDOS (red) plots for the triclinic **A:4** cocrystal. The PDOS plot shows the contribution of coformer molecule to the total DOS. The HOCO (99) and LUCO (100) bands are marked with blue rectangles. It is evident that these bands are almost entirely localized on molecules **A.**

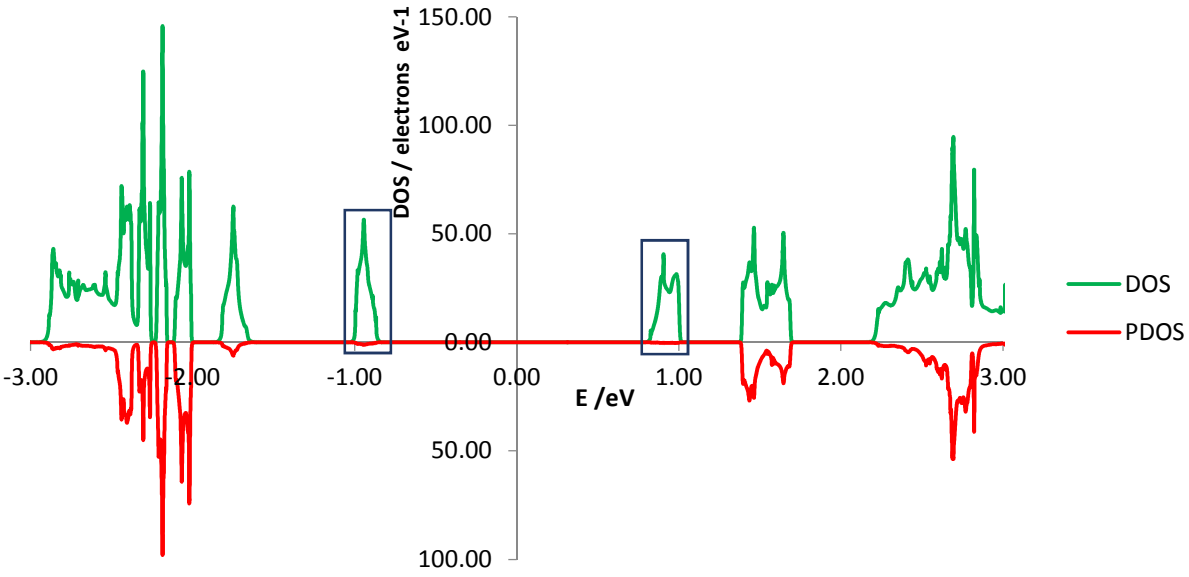

Figure S10. DOS (green) and PDOS (red) plots for the monoclinic structure of **A:4** cocrystal. The PDOS plot shows the contribution of coformer molecule to the total DOS. The pairs of nearly degenerate HOCO (197, 198) and LUCO (199, 200) bands are marked with blue rectangles. It is evident that these bands are almost entirely localized on molecules **A.**

1.4 Band structure calculations

Band structure calculation was performed using the PBE functional with 0.015 $Å^{-1}$ k-point spacing. Band dispersion was computed along the following k-point path:

1. 0, 0, 0
2. ½, 0, 0
3. ½, ½, 0
4. 0, ½, 0
5. 0, ½, ½
6. ½, ½, ½
7. ½, 0, ½
8. 0, 0, ½
9. 0, 0, 0

The band structure plots are shown in Figures S11-S18. Each plot shows the 10 highest occupied and 10 lowest unoccupied electronic bands.

In addition to the plane-wave calculations, band structures for the triclinic and monoclinic structures of the cocrystals were calculated in the code CRYSTAL14[13] using a localized TZVP basis set specially modified for periodic calculations.[14] Localized basis sets are more suitable for calculations with hybrid DFT functionals, therefore CRYSTAL calculations were used to calculate band structure plots with B3LYP functional and compare it with the PBE band structures. The results of these calculations are shown in figures S19-S25 and Table S31.

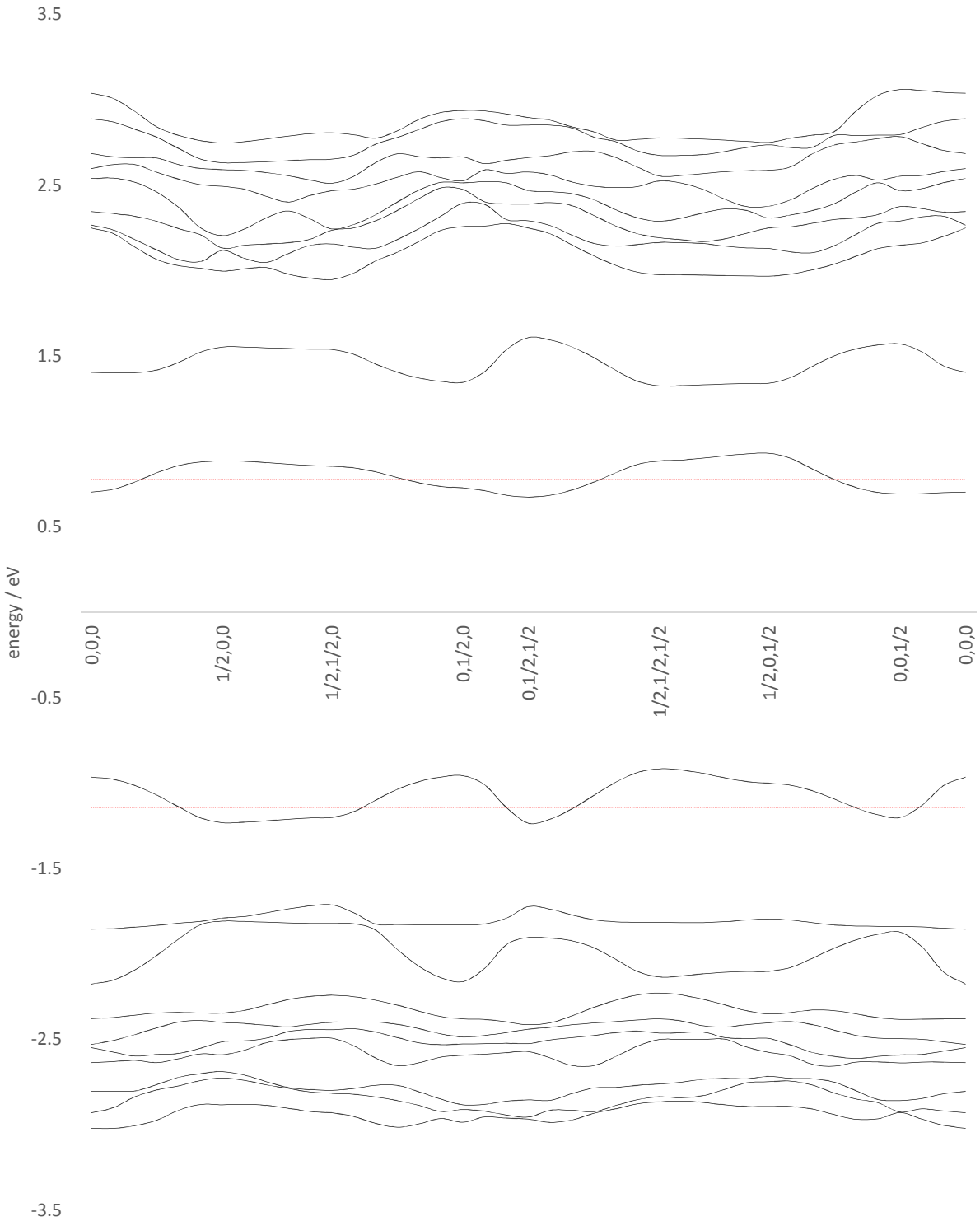

Figure S11. Band structure plot for the triclinic structure of the **A:1** cocrystal. Bands ranging from HOCO-9 to LUCO+9 are shown. The dashed red lines represent the energies of the HOCO and LUCO bands at the mean-value k-point.

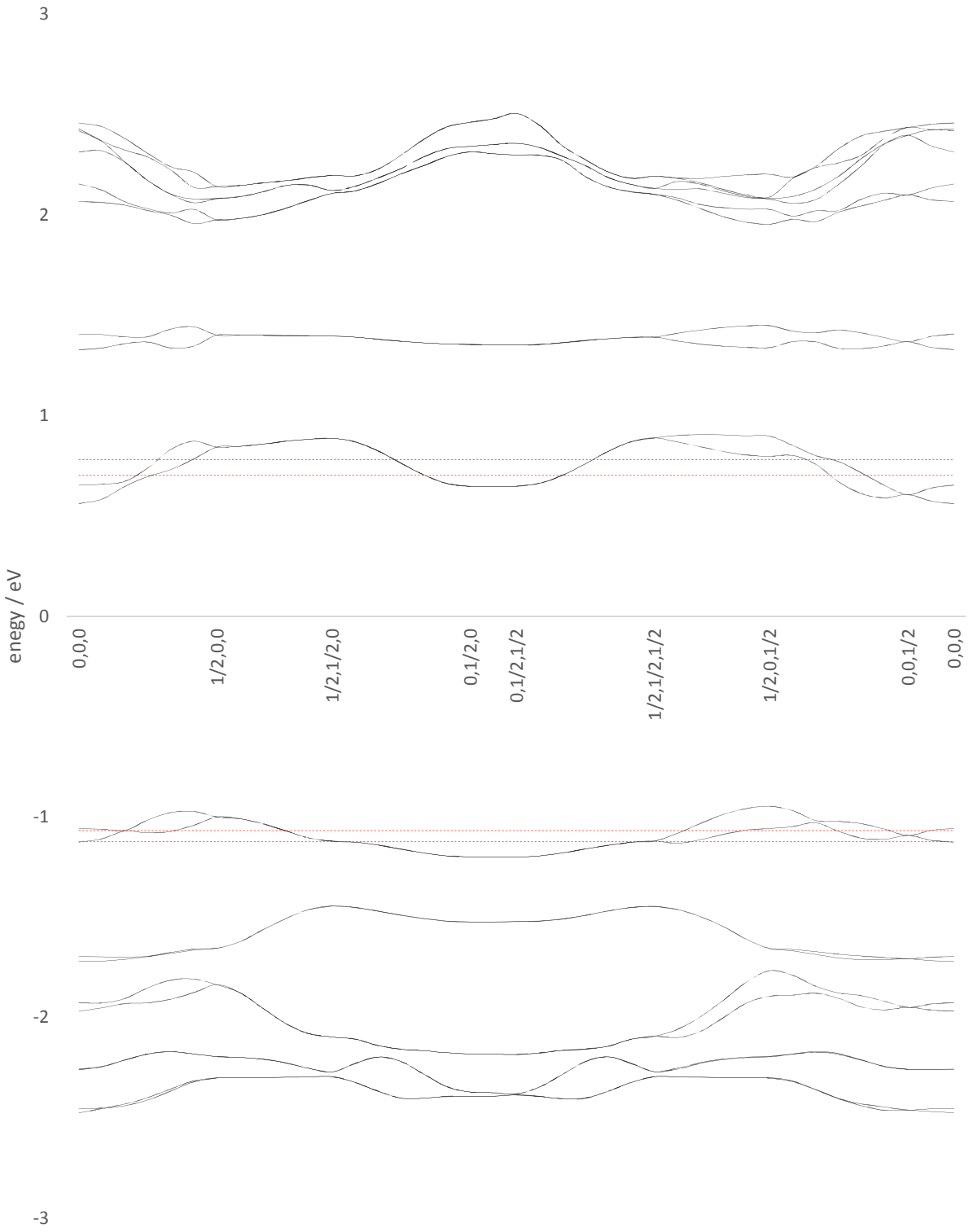

Figure S12. Band structure plot for the monoclinic structure of the **A:1** cocrystal. Bands ranging from HOCO-9 to LUCO+9 are shown. The dashed red lines represent the energies of the (HOCO-1, HOCO) and (LUCO, LUCO+1) band pairs at the mean-value k-point.

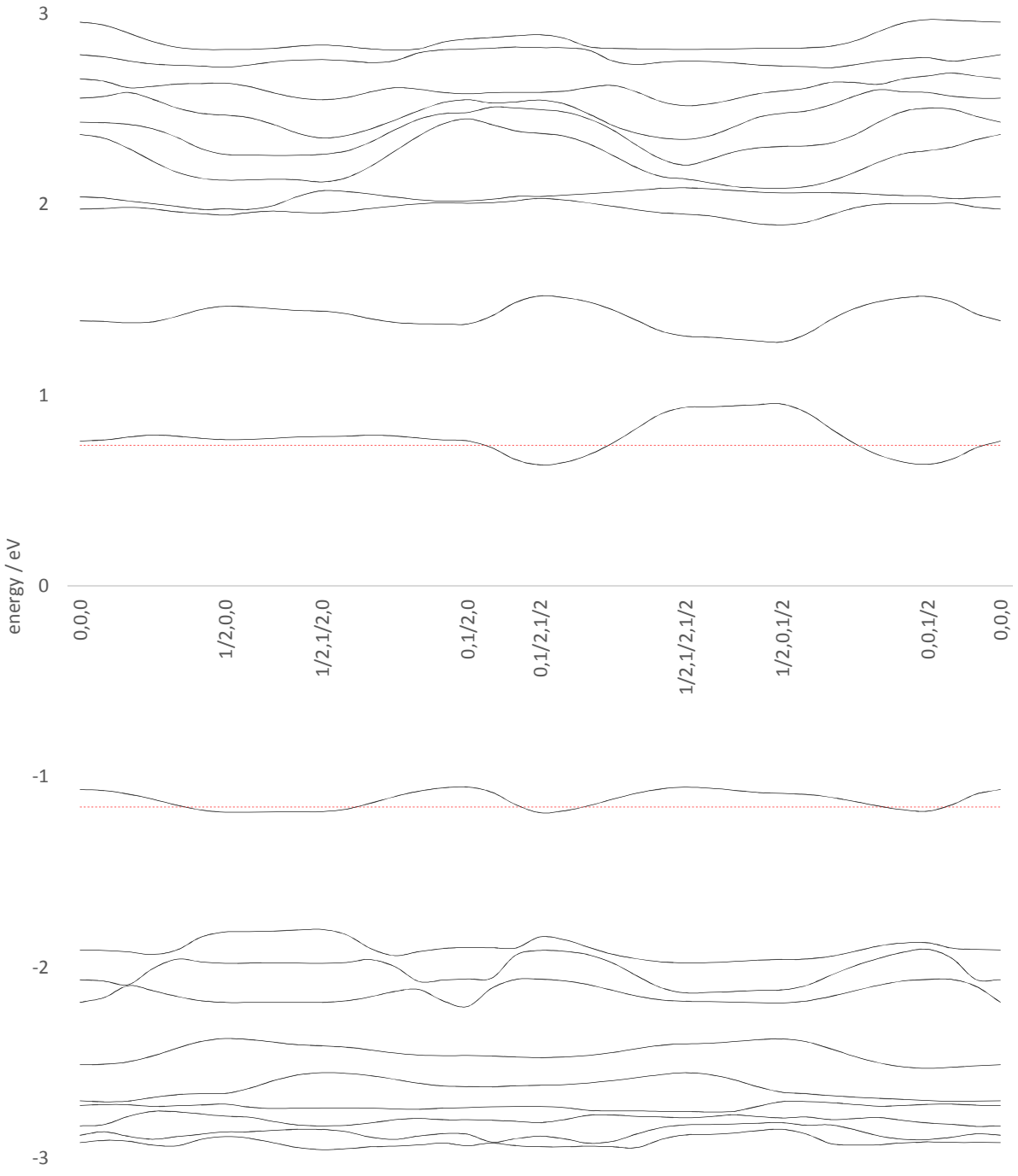

Figure S13. Band structure plot for the triclinic structure of the **A:2** cocrystal. Bands ranging from HOCO-9 to LUCO+9 are shown. The dashed red lines represent the energies of the HOCO and LUCO bands at the mean-value k-point.

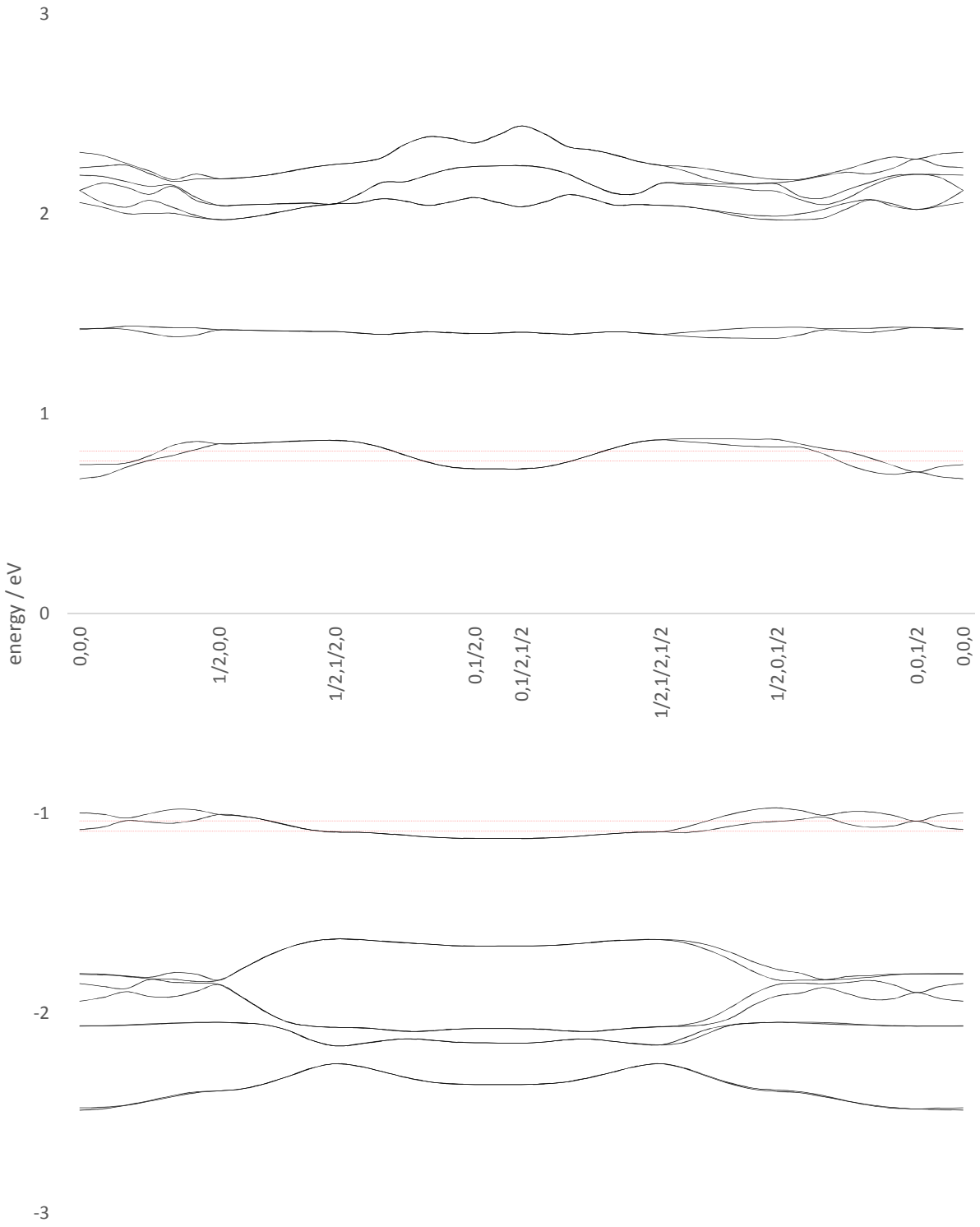

Figure S14. Band structure plot for the monoclinic structure of the **A:2** cocrystal. Bands ranging from HOCO-9 to LUCO+9 are shown. The dashed red lines represent the energies of the (HOCO-1, HOCO) and (LUCO, LUCO+1) band pairs at the mean-value k-point.

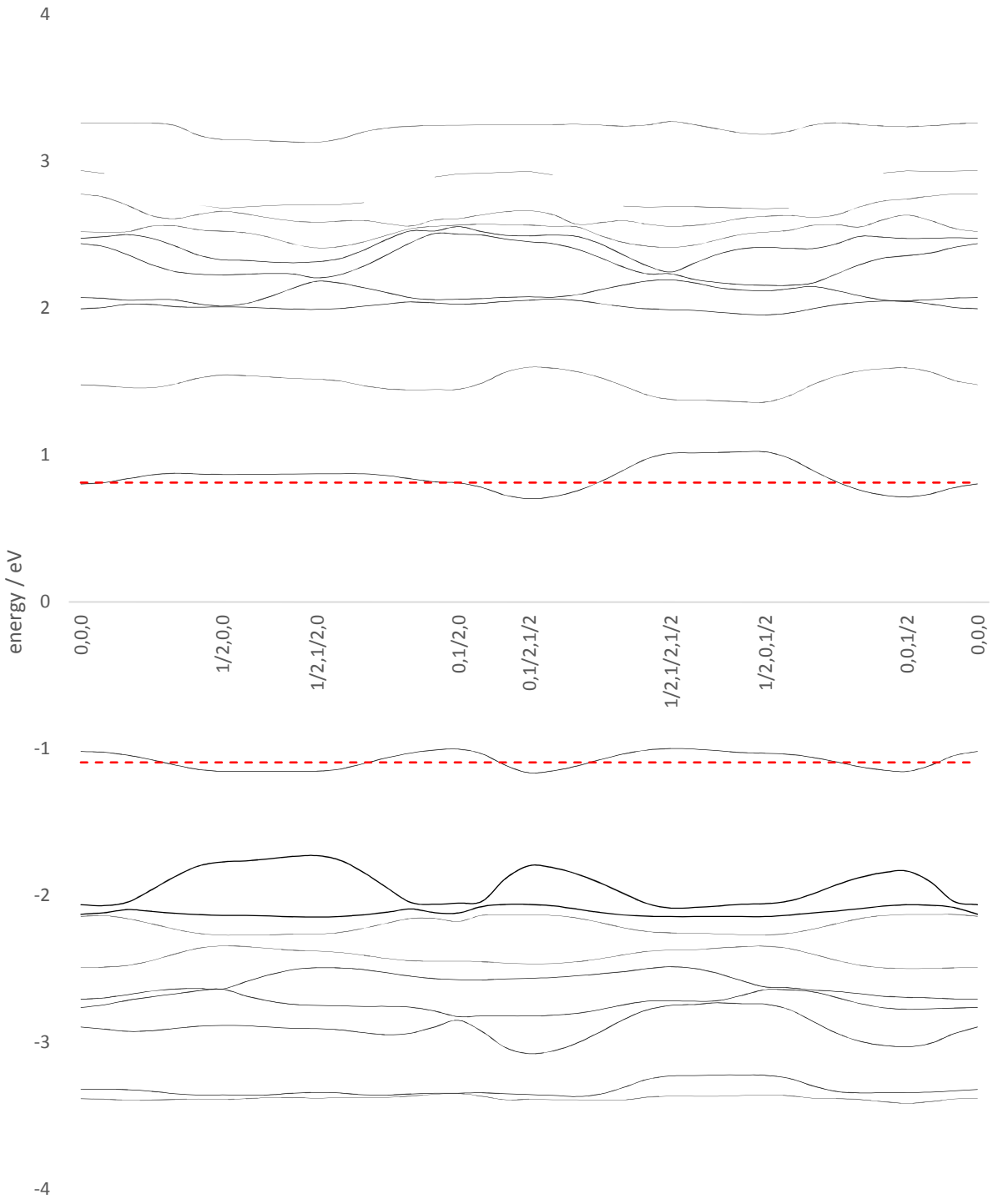

Figure S15. Band structure plot for the triclinic structure of the **A:3** cocrystal. Bands ranging from HOCO-9 to LUCO+9 are shown. The dashed red lines represent the energies of the HOCO and LUCO bands at the mean-value k-point.

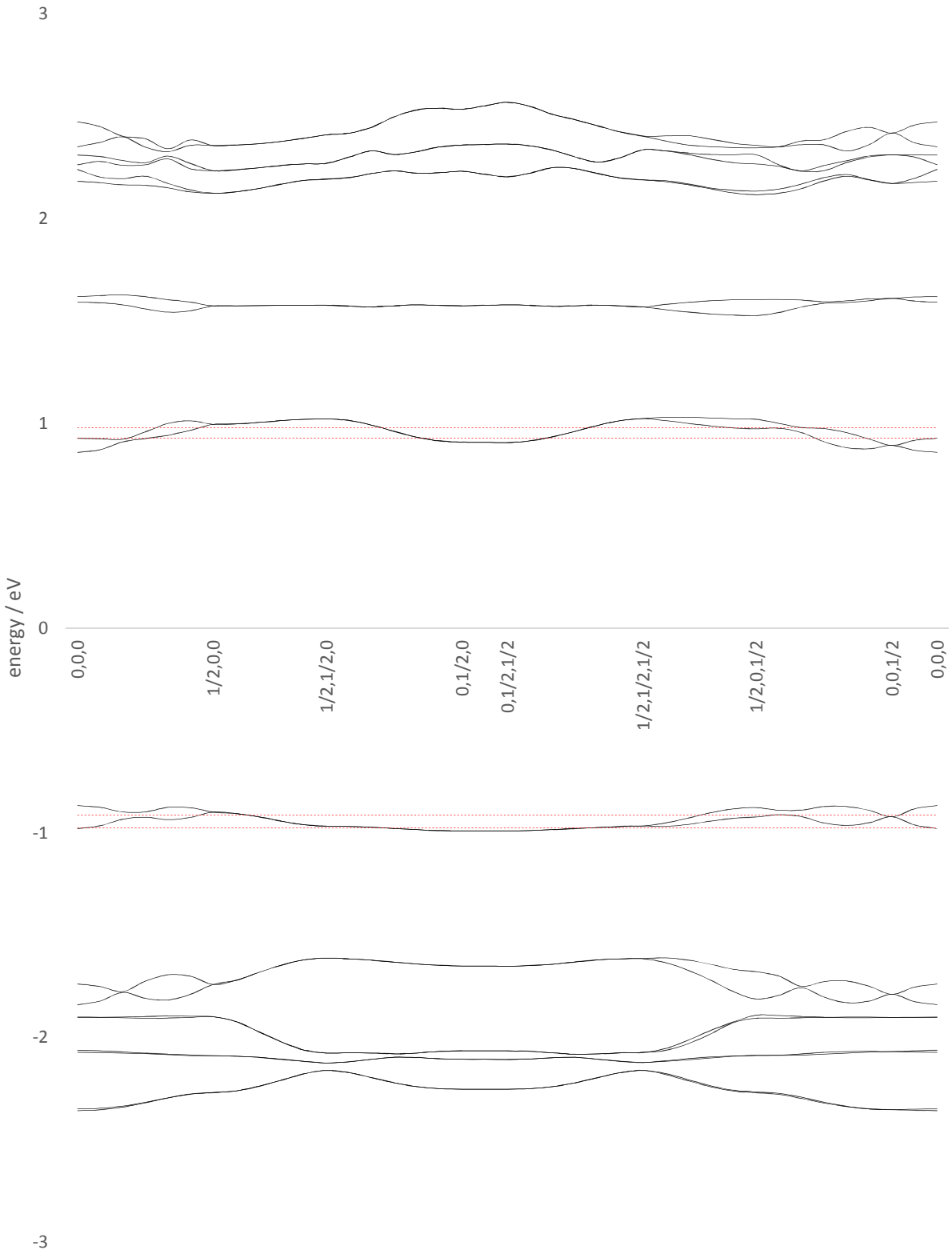

Figure S16. Band structure plot for the monoclinic structure of the **A:3** cocrystal. Bands ranging from HOCO-9 to LUCO+9 are shown. The dashed red lines represent the energies of the (HOCO-1, HOCO) and (LUCO, LUCO+1) band pairs at the mean-value k-point.

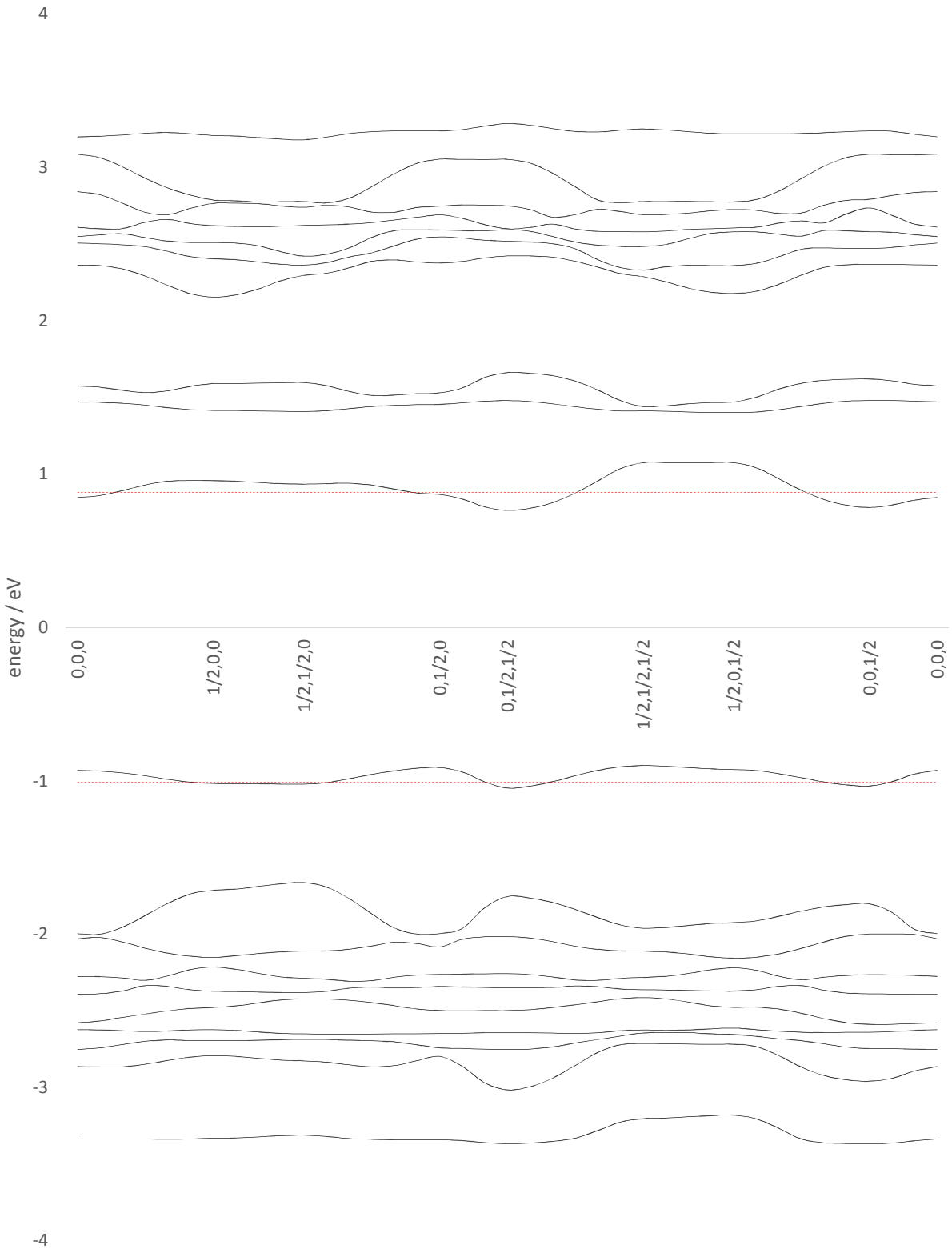

Figure S17. Band structure plot for the triclinic structure of the **A:4** cocrystal. Bands ranging from HOCO-9 to LUCO+9 are shown. The dashed red lines represent the energies of the HOCO and LUCO bands at the mean-value k-point.

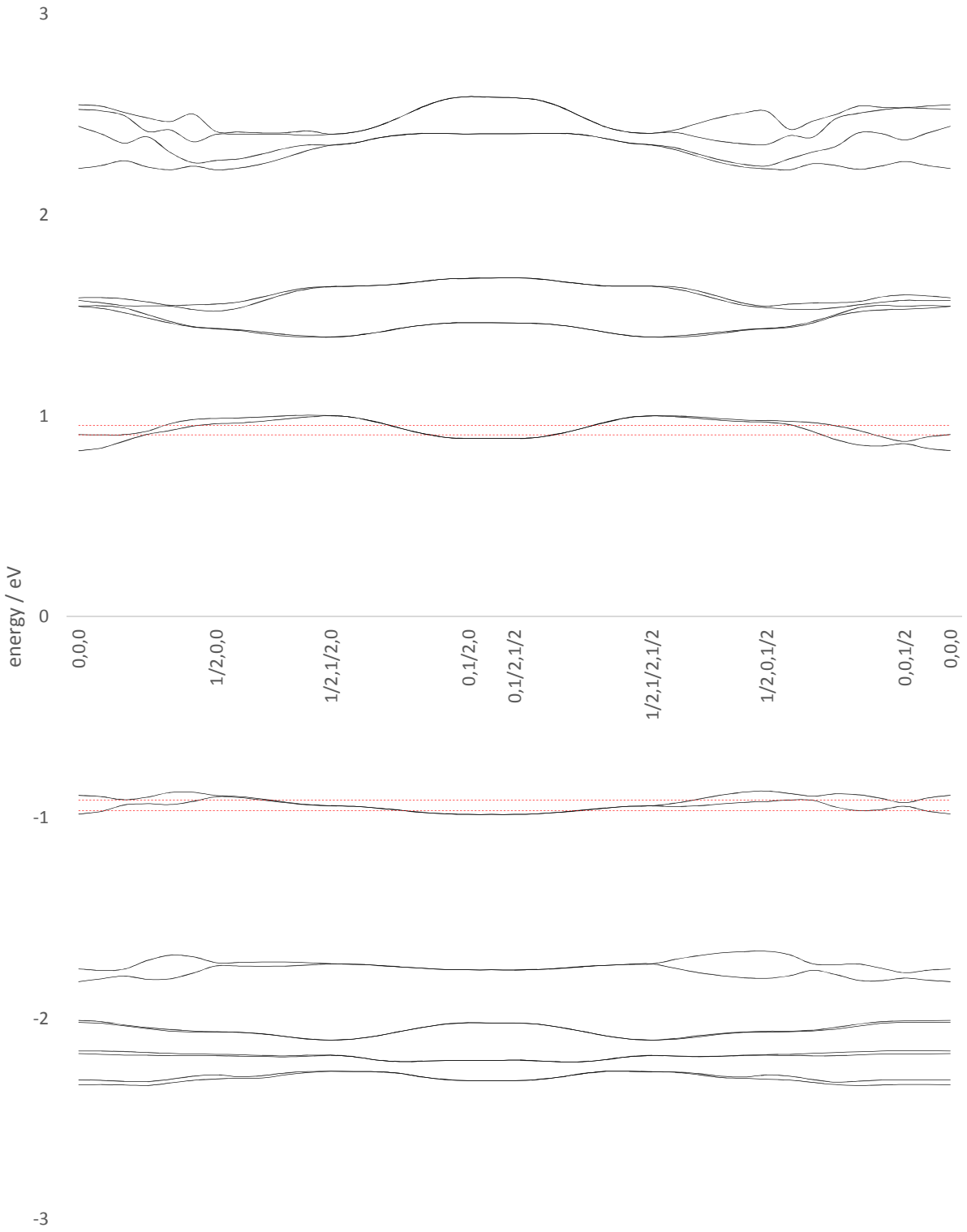

Figure S18. Band structure plot for the monoclinic structure of the **A:4** cocrystal. Bands ranging from HOCO-9 to LUCO+9 are shown. The dashed red lines represent the energies of the (HOCO-1, HOCO) and (LUCO, LUCO+1) band pairs at the mean-value k-point.

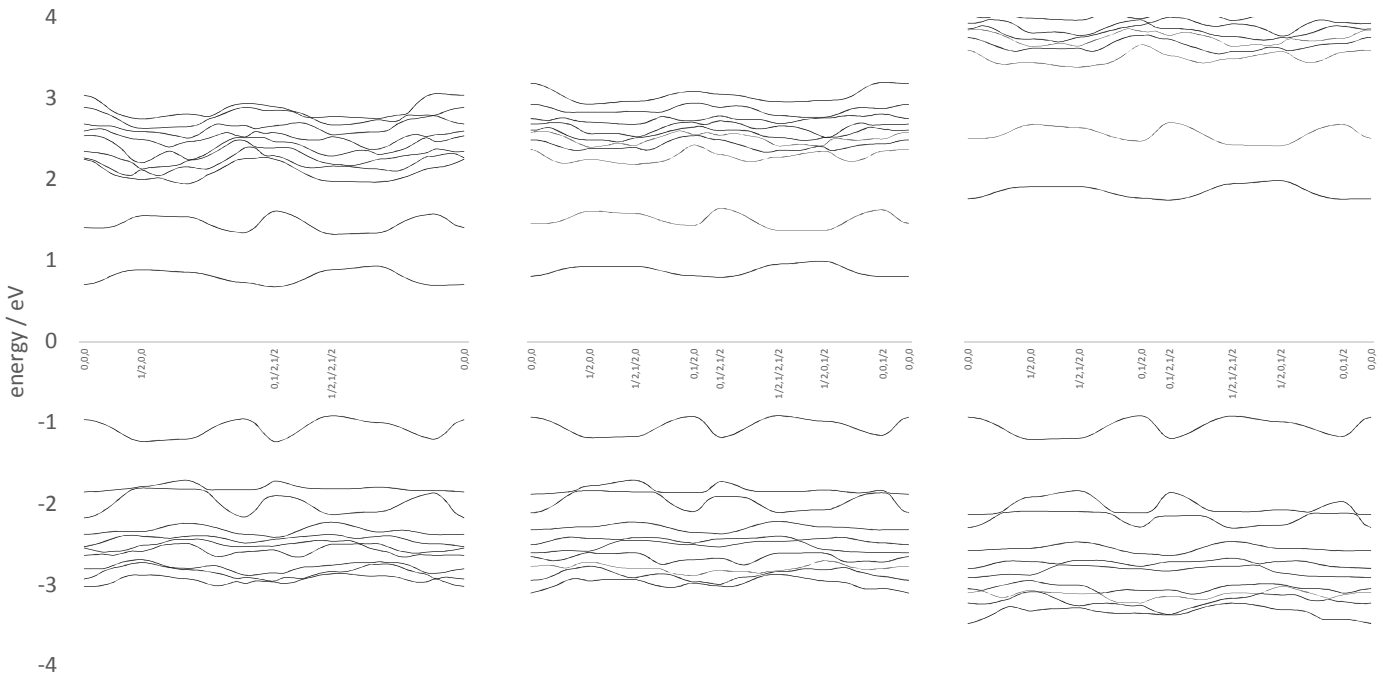

Figure S19. Band structure plots for the triclinic structure of the **A:1** cocrystal. From left to right: BS calculated with PBE functional using plane-wave basis set in CASTEP, BS calculated with PBE functional using TZVP localized basis set in CRYSTAL and BS calculated with B3LYP functional using TZVP localized basis set in CRYSTAL. The PBE BS plots calculated using plane-wave and TZVP basis sets are in good agreement. The B3LYP band structure shows a larger band gap.

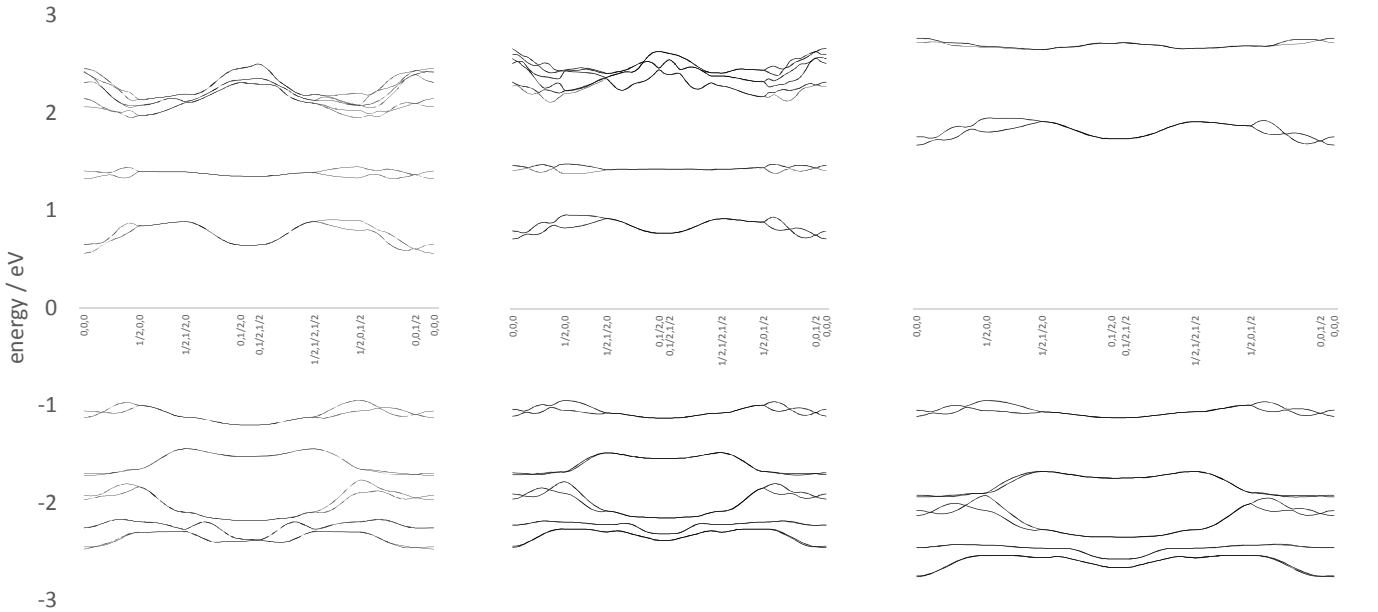

Figure S20. Band structure plots for the monoclinic structure of the **A:1** cocrystal. From left to right: BS calculated with PBE functional using plane-wave basis set in CASTEP, BS calculated with PBE functional using TZVP localized basis set in CRYSTAL, BS calculated with B3LYP functional using TZVP localized basis set in CRYSTAL. The PBE BS plots calculated using plane-wave and TZVP basis sets are in good agreement. The B3LYP band structure shows a larger band gap.

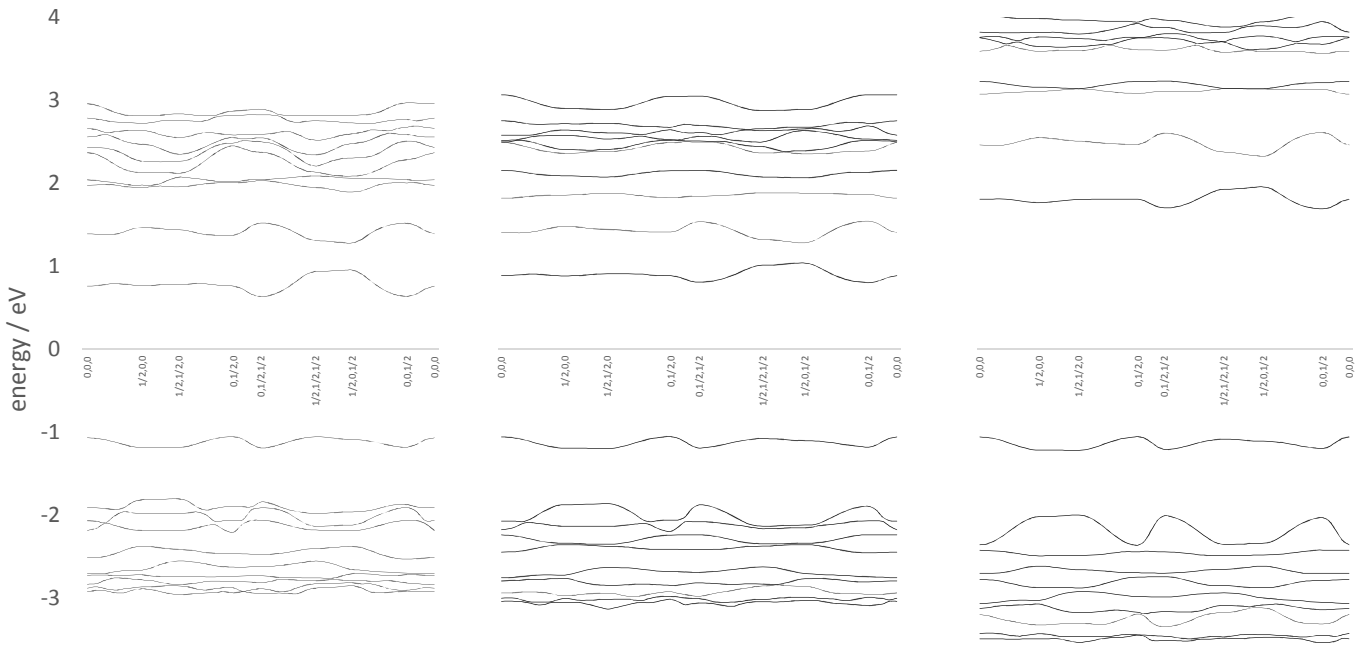

Figure S21. Band structure plots for the triclinic structure of the **A:2** cocrystal. From left to right: BS calculated with PBE functional using plane-wave basis set in CASTEP, BS calculated with PBE functional using TZVP localized basis set in CRYSTAL, BS calculated with B3LYP functional using TZVP localized basis set in CRYSTAL. The PBE BS plots calculated using plane-wave and TZVP basis sets are in good agreement. The B3LYP band structure shows a larger band gap.

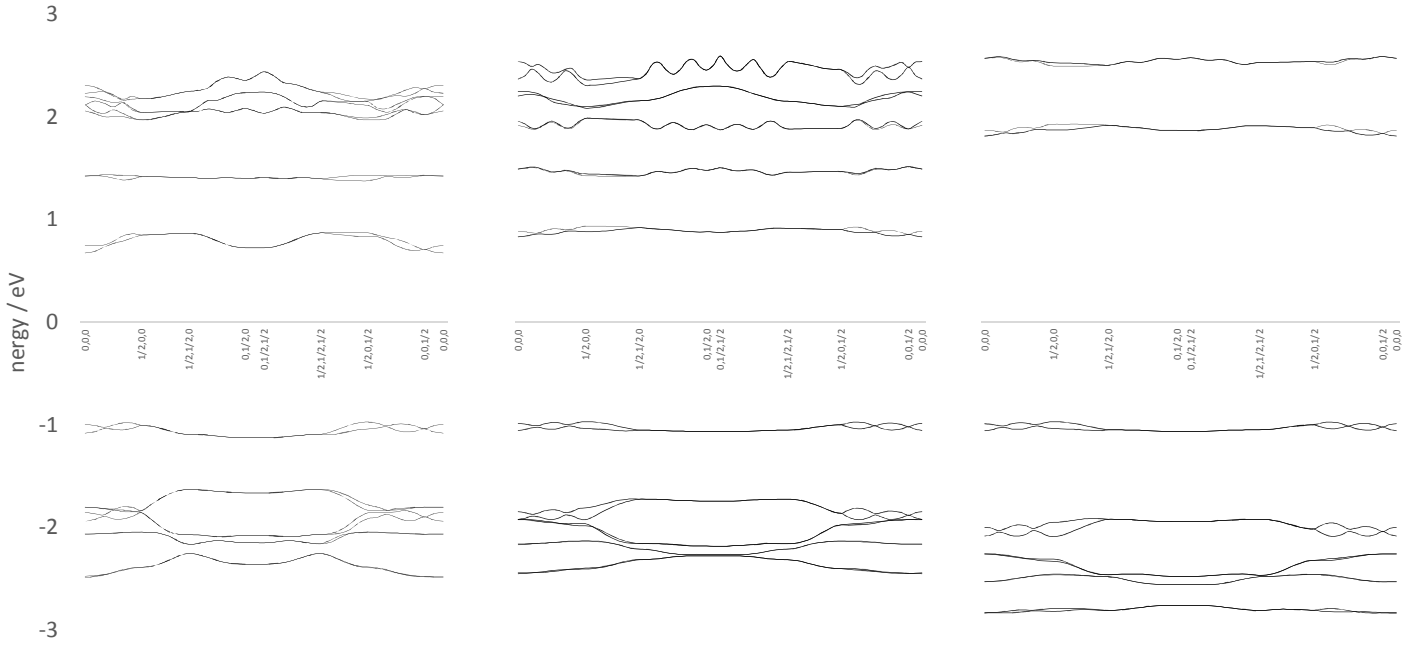

Figure S22. Band structure plots for the monoclinic structure of the **A:2** cocrystal. From left to right: BS calculated with PBE functional using plane-wave basis set in CASTEP, BS calculated with PBE functional using TZVP localized basis set in CRYSTAL, BS calculated with B3LYP functional using TZVP localized basis set in CRYSTAL. The PBE BS plots calculated using plane-wave and TZVP basis sets are in good agreement. The B3LYP band structure shows a larger band gap.

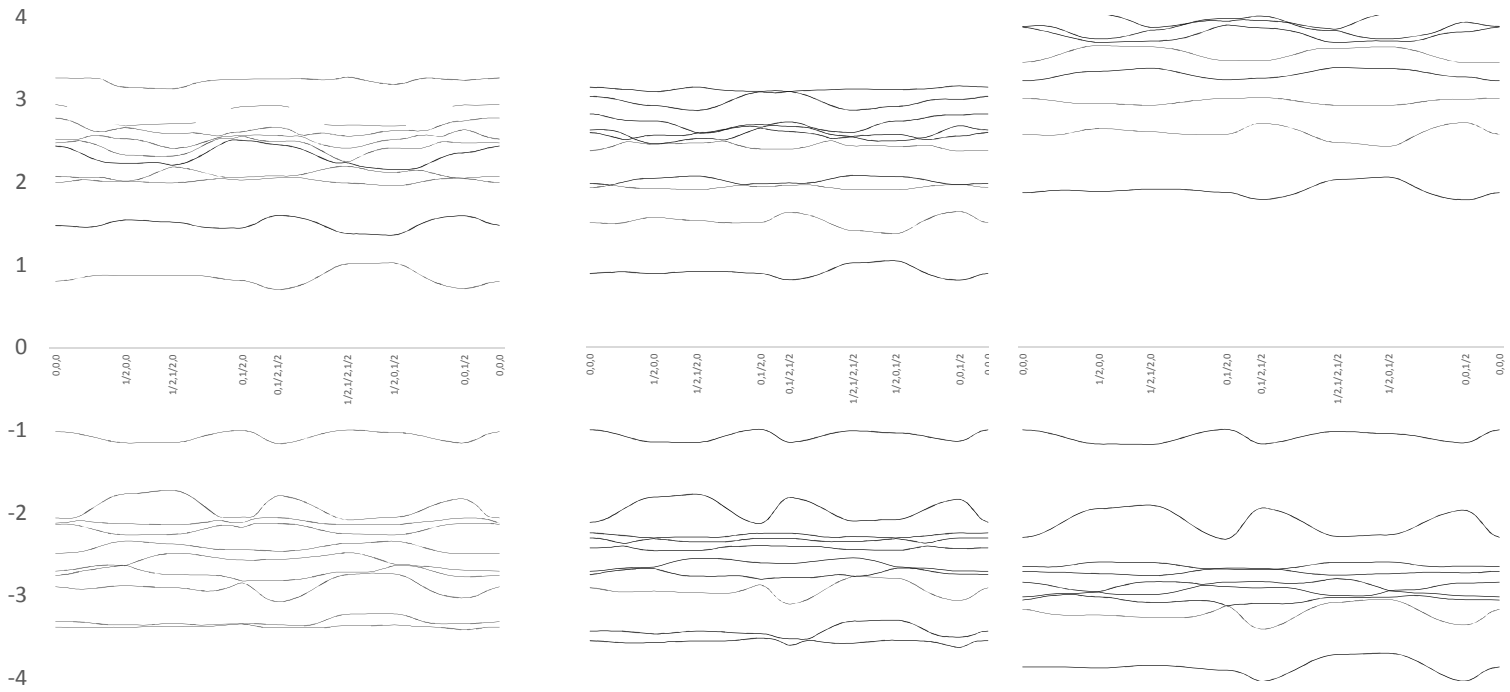

Figure S23. Band structure plots for the triclinic structure of the **A:3** cocrystal. From left to right: BS calculated with PBE functional using plane-wave basis set in CASTEP, BS calculated with PBE functional using TZVP localized basis set in CRYSTAL, BS calculated with B3LYP functional using TZVP localized basis set in CRYSTAL. The PBE BS plots calculated using plane-wave and TZVP basis sets are in good agreement. The B3LYP band structure shows a larger band gap.

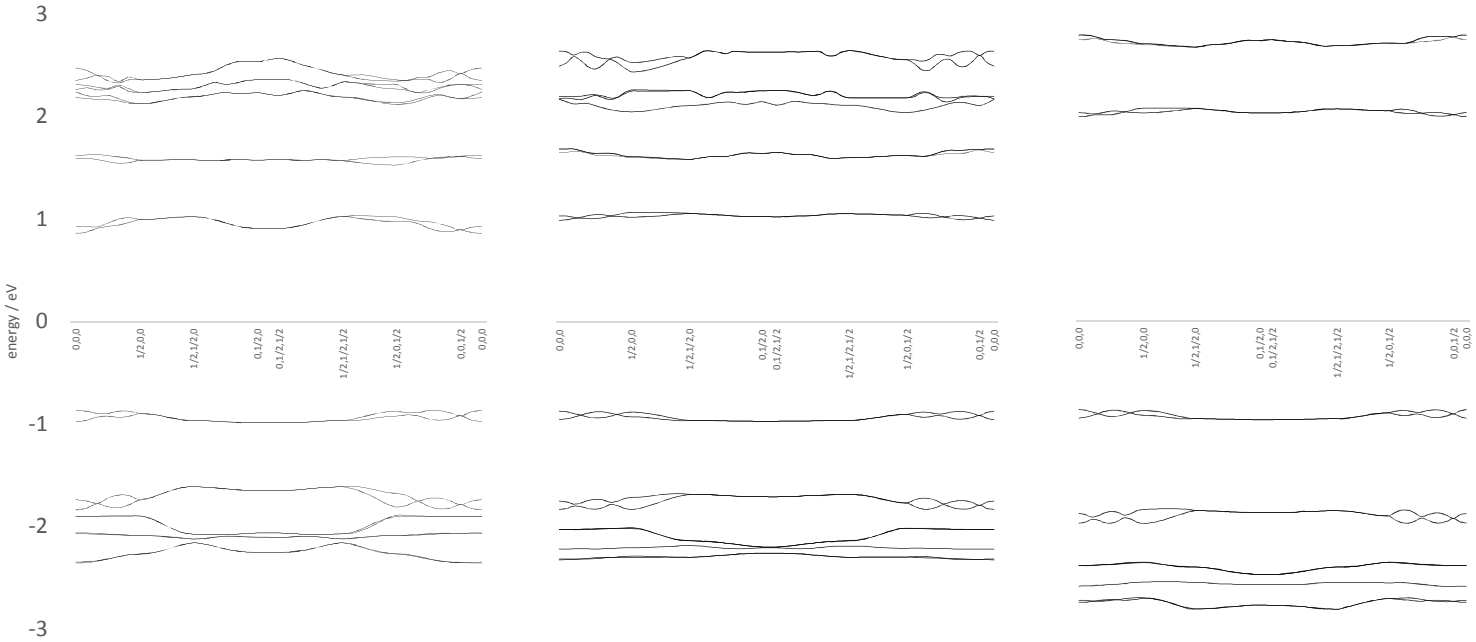

Figure S24. Band structure plots for the monoclinic structure of the **A:3** cocrystal. From left to right: BS calculated with PBE functional using plane-wave basis set in CASTEP, BS calculated with PBE functional using TZVP localized basis set in CRYSTAL, BS calculated with B3LYP functional using TZVP localized basis set in CRYSTAL. The PBE BS plots calculated using plane-wave and TZVP basis sets are in good agreement. The B3LYP band structure shows a larger band gap.

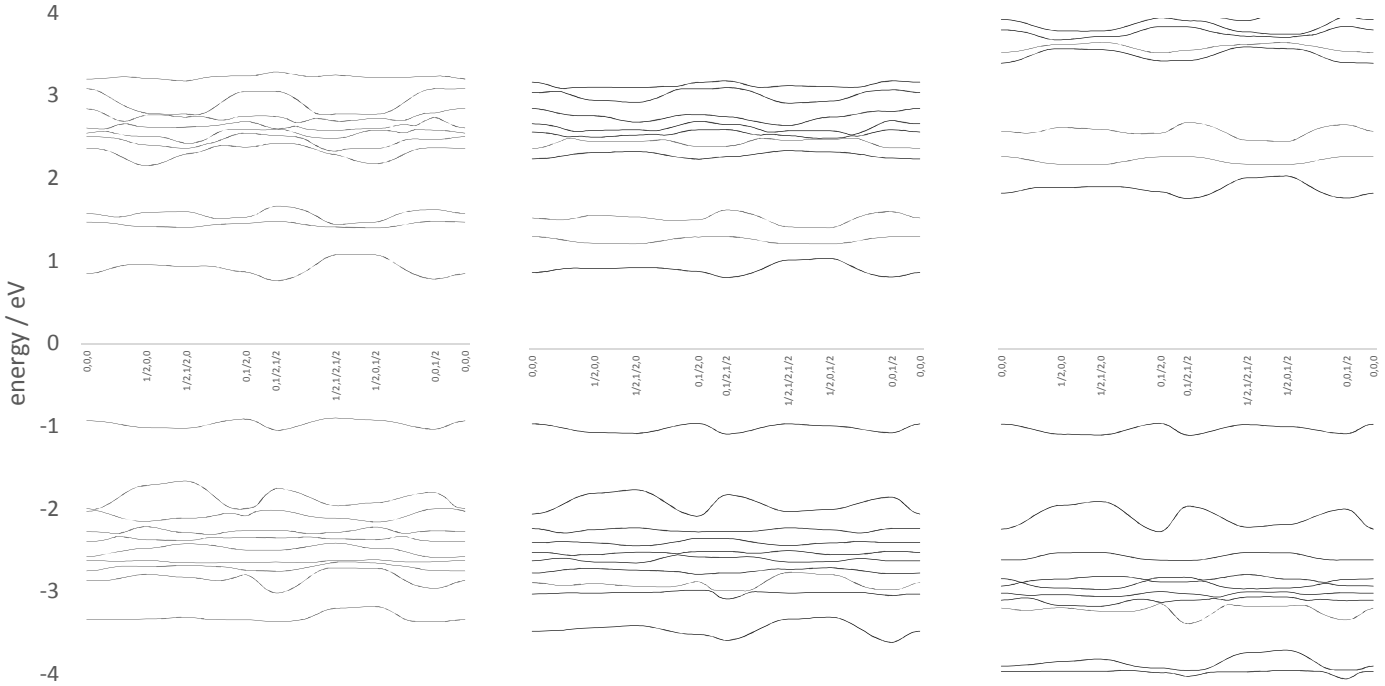

Figure S25. Band structure plots for the triclinic structure of the **A:4** cocrystal. From left to right: BS calculated with PBE functional using plane-wave basis set in CASTEP, BS calculated with PBE functional using TZVP localized basis set in CRYSTAL, BS calculated with B3LYP functional using TZVP localized basis set in CRYSTAL. The PBE BS plots calculated using plane-wave and TZVP basis sets are in good agreement. The B3LYP band structure shows a larger band gap.

.

Table S31. Comparison of calculated band gaps. CASTEP-PBE band gaps are approx. 0.1 eV lower than PBE band gaps calculated in CRYSTAL. The difference between PBE and B3LYP band gaps is 0.95-1 eV for all crystal structures, both triclinic and monoclinic. The B3LYP band gaps also compare favorably to the TD-DFT energy for excited state S_1

Cocrystal		Band gap / eV			TD-DFT B3LYP energy of the S_1 excited state	CRYSTAL B3LYP-PBE band gap difference
		CASTEP PBE	CRYSTAL PBE	CRYSTAL B3LYP		
A:1	triclinic	1.591	1.706	2.661	2.667	0.955
	monoclinic	1.508	1.657	2.620	2.623	0.963
A:2	triclinic	1.689	1.782	2.746	2.514	0.963
	monoclinic	1.647	1.801	2.784	2.625	0.982
A:3	triclinic	1.701	1.801	2.770	2.562	0.969
	monoclinic	1.725	1.859	2.852	2.663	0.993
A:4	triclinic	1.663	1.766	2.721	2.501	0.955
	monoclinic	1.694	-	-	2.650	-

2. Calculation of fluorescence spectra for molecules in the gas phase.

Emission spectra for molecule **A** was calculated with GAUSSIAN16 software. Calculations were performed at TD-DFT/B3LYP level of theory using 6-311G(d,p) basis set. First geometry optimizations were performed for the DFT ground state and TD-DFT S_1 excited state. Then vibrational frequency calculations were performed for both electronic states in their optimized geometries. Finally, Franck-Condon factors for electronic-vibrational transitions were calculated.

References

(1) Clark, S. J.; Segall, M. D.; Pickard, C. J.; Hasnip, P. J.; Probert, M. I. J.; Refson, K.; Payne, M. C. First Principles Methods Using CASTEP. *Z. Kristallogr.*. **2005**, *220*, 567–570.

(2) Rappe, A. M.; Rabe, K. M.; Kaxiras, E.; Joannopoulos, J. D. Optimized Pseudopotentials. *Phys. Rev. B* **1990**, *41*, 1227–1230.

(3) Yan, D.; Delori, A.; Lloyd, G. O.; Friščić, T.; Day, G. M.; Jones, W.; Lu, J.; Wei, M.; Evans, D. G.; Duan, X. A Cocrystal Strategy to Tune the Luminescent Properties of Stilbene-Type Organic Solid-State Materials. *Angew. Chem. Int. Ed.* **2011**, *50*, 12483–12486.

(4) Monkhorst, H. J.; Pack, J. D. Special Points for Brillouin-Zone Integrations. *Phys. Rev. B* **1976**, *13*, 5188–5192.

(5) Grimme, S. Semiempirical GGA-Type Density Functional Constructed with a Long-Range Dispersion Correction. *J. Comput. Chem.* **2006**, *27*, 1787–1799.

(6) Baldereschi, A. Mean-Value Point in the Brillouin Zone. *Phys. Rev. B* **1973**, *7*, 5212–5215.

(7) Magyar, R. J.; Tretiak, S. Dependence of Spurious Charge-Transfer Excited States on Orbital Exchange in TDDFT: Large Molecules and Clusters. *J. Chem. Theory Comput.* **2007**, *3*, 976–987.

(8) Dreuw, A.; Weisman, J. L.; Head-Gordon, M. Long-Range Charge-Transfer Excited States in Time-Dependent Density Functional Theory Require Non-Local Exchange. *J. Chem. Phys.* **2003**, *119*, 2943–2946.

(9) Tozer, D. J. Relationship between Long-Range Charge-Transfer Excitation Energy Error and Integer Discontinuity in Kohn-Sham Theory. *J. Chem. Phys.* **2003**, *119*, 12697–12699.

(10) Morris, A. J.; Nicholls, R. J.; Pickard, C. J.; Yates, J. R. OptaDOS: A Tool for Obtaining Density of States, Core-Level and Optical Spectra from Electronic Structure Codes. *Comput. Phys. Commun.* **2014**, *185*, 1477–1485.

(11) Nicholls, R. J.; Morris, A. J.; Pickard, C. J.; Yates, J. R. OptaDOS - a New Tool for EELS

Calculations. *J. Phys. Conf. Ser.* **2012**, *371*, 012062.

(12) Yates, J. R.; Wang, X.; Vanderbilt, D.; Souza, I. Spectral and Fermi Surface Properties from Wannier Interpolation. *Phys. Rev. B* **2007**, *75*, 195121.

(13) Dovesi, R.; Orlando, R.; Erba, A.; Zicovich-Wilson, C. M.; Civalleri, B.; Casassa, S.; Maschio, L.; Ferrabone, M.; De La Pierre, M.; D'Arco, P.; et al. CRYSTAL14 : A Program for the *Ab Initio* Investigation of Crystalline Solids. *Int. J. Quantum Chem.* **2014**, *114*, 1287–1317.

(14) Peintinger, M. F.; Vilela Oliveira, D.; Bredow, T. Consistent Gaussian Basis Sets of Triple-Zeta Valence with Polarization Quality for Solid-State Calculations. *J. Comput. Chem.* **2013**, *34*, 451–459.